

Department of Companion Animals and Horses  
University of Veterinary Medicine Vienna

Clinical Unit of Diagnostic Imaging  
(Head: Univ.-Prof. Dr.med.vet. Eberhard Ludewig Dipl. ECVDI)

**Radiographic and CT findings and course of disease  
in two severe cases of metabolic bone disease in  
subadult black and white tegus (*Tupinambis  
merianae*). Case report.**

Diplomarbeit

University of Veterinary Medicine Vienna

Submitted by  
Julia Ulrich

Vienna, July 2022

**Supervisor**

Ass.-Prof. Dr. Michaela Gumpenberger

**Gutachter**

Dr. Jean Meyer, Univ.-Lektor

## **Table of content**

1. Introduction
2. Materials and methods
3. General results
4. Case report A
  - 4.1. Animal data, medical history
  - 4.2. Clinical examination
  - 4.3. Diagnostic imaging
  - 4.4. Therapy, course of disease
5. Case report B
  - 5.1. Animal data, medical history
  - 5.2. Clinical examination, laboratory diagnostics
  - 5.3. Diagnostic imaging
  - 5.4. Therapy, course of disease
6. Discussion
7. Zusammenfassung
8. Summary
9. Abbreviations
10. Bibliography
11. List of figures/tables

## 1. Introduction

The following case report describes the long-term radiographic and CT documentation of two black and white tegus (*Tupinambis merianae*) that presented with severe clinical symptoms of metabolic bone disease (MBD).

A number of bone disorders have already been described for reptiles in captive care, with their clinical relevance sometimes differing drastically. Nutritional secondary hyperparathyroidism is hereby the most common cause of MBD due to long-term dietary deficiency of calcium and/or of vitamin D, a negative calcium-phosphorus (Ca : P) ratio and/or lack of sufficient UV-B light (Rendle and Calvert 2019). Other nutritional and housing-related MBDs (osteomalacia, osteoporosis, fibrous osteodystrophy) especially in connection with various clinical presentations of hypocalcemia, play a major role in reptile medicine. On the other hand rare skeletal diseases such as hypertrophic osteopathy (Barten 2000), osteopetrosis (Ocarino et al. 2008, Reece et al. 1986) and osteitis deformans (Preziosi et al. 2007) have only been documented in few cases.

Typical clinical findings for NSHP in reptiles have been described many times and include anorexia, weight loss, muscular tremors in lizards, deformed limbs, inability to lift the trunk off the ground, lameness, preovulatory follicular stasis and dystocia, scoliosis, kyphosis, pliable mandibles or maxillae, swelling of the limbs, painful limbs, constipation and paralysis of the hind limbs (Rendle and Calvert 2019, Klaphake 2010, Hoby et al. 2010). Common radiographic findings of NSHP in reptiles include soft tissue thickening, generally decreased bone opacity, periosteal reactions, folding fractures in juveniles, pathologic fractures in adults, enlarged and distorted costo-chondral junctions (rachitic rosettes) and long bone bowing (Rendle and Calvert 2019, Williams 2002, Silverman 2006). However, controversial arguments exist about thinning or even thickening of the long bone cortices during the course of illness (Zotti et al. 2004, Rendle and Calvert 2019, Carmel and Johnson 2018, Boyer and Scott 2019). These skeletal changes often remain subclinical for a long time in mild and moderate stages and experience has shown that they therefore may go unnoticed by the animal owner and even veterinarian. For this reason, it is recommended to always assess the overall skeletal system in general and bone density in particular whenever doing radiographs, regardless of the reason of presentation (Pees 2010a). However, radiography is a quite imprecise diagnostic method to grade mineral

deficiencies, especially for the early detection of changes in the density of the skeleton, as it only shows recognizable changes from a mineralization loss of 30-60 % (Dennis et al. 2001). CT on the other hand is not compromised by superimposition and is therefore superior to detect even slight changes in bone density or new bone tissue formation as well as changes in density of soft tissue (mineralizations) (Kiefer and Pees 2010, Raiti and Haramati 1997).

## 2. Materials and Methods

For a retrospective, descriptive case series study, CT images and radiographs of nine black and white tegus (*Tupinambis merianae*) and one red tegu (*Tupinambis rufescens*) were reevaluated. Five females between nine months and two years and three months and five males between the ages of four and eight years were included in the study. To evaluate each individual's physical state of development, data available in current species-specific literature, assuming an average hatching weight of 20g and an average weight of up to 1500g (females a little less than males) after the first 12 months, as well as the observed onset of sexual maturity (oviposition in the female animals) which usually occurs at the age of two to two and a half years in good captive care (Köhler and Langerwerf 2000) were used.

Of the ten animals, three were from zoological facilities and seven from private collections. CT images and radiographs of six animals were obtained at the Clinical Unit of Diagnostic Imaging of the University of Veterinary Medicine Vienna due to various medical indications. Radiographs of four animals were transmitted in DICOM format with requests for further diagnosis from external veterinarians.

Available data concerning species, age and sex of each animal at first presentation were documented as well as basic husbandry and dietary parameters and the reason for initial presentation. These data are summarized in table 1.

Tab. 1. Animal data of nine black and white tegu (*Tupinambis merianae*) (BW tegu) and one red tegu (*Tupinambis rufescens*) (R tegu) at initial presentation.

ID	1	2	3	4	5	6	7	8	9	10
Species	BW tegu	BW tegu	BW tegu	BW tegu	BW tegu	BW tegu	BW tegu	BW tegu	BW tegu	R tegu
Sex	female	female	female	male	female	female	male	male	male	male
Age at presentation	9m	1y 11m	1y 11m	4y	1y	2y 3m	6y	7y	8y	8y
Weight (g)	1058	1745	848	7620	1170	1546	6200	6550	6872	7000
Private keeping/ zoological institute	private	private	private	private	private	private	zoo	zoo	zoo	private
Origin	FB	CB	FB	unknown	unknown	FB	unknown	unknown	unknown	unknown
Diet*	fuzzy mice, raw chicken, beef and pork	varied diet	fuzzy mice	varied diet	varied diet	varied diet	varied diet	varied diet	varied diet	varied diet
Ca-Supplementation	no	yes	no information available	yes	yes	yes	yes	yes	yes	yes
Product/Products	-	Miner-All Indoor	-	-	-	herpetal Complete T	herpetal Complete T	herpetal Complete T	herpetal Complete T	-
Frequency	-	once a week	-	once a week	-	twice a week	irregularly	irregularly	irregularly	-
Amount per use (g)	-	-	-	-	-	0.7	-	-	-	-
UV-B provided	yes	yes	no information available	yes	yes	yes	yes	yes	yes	yes
Product(s)	no information available	1x Lucky Reptile Bright Sun FLOOD Desert 70W  1 x Reptiles Expert UVB 100 W Spot	-	no information available	no information available	2x Reptiles Expert UVB 70 W Flood	1x JBL UV-Spot Plus 100 W  1x Osram Ultra Vitalux 300 W	2x Osram Ultra Vitalux 300 W	2x Osram Ultra Vitalux 300 W	no information available
Exposure time per day (h)	-	summer: 12 winter: 10	-	-	-	summer: 12 winter: 10	summer: 12 h / 3h winter: 10h / 3h	summer: 3 winter: 3	summer: 3 winter: 3	-
UVI	-	UVI 4.1 / 4.7	-	-	-	UVI 5.1 / 4.9	UVI 5.0 / 6.1	UVI 5.8 / 5.6	UVI 5.3 / 5.7	-
Last replacement	4 months ago	4 months ago	-	-	-	2 months ago	3 months ago	4 months ago	4 months ago	-
Reason of presentation	Bump on the ribs	Femur fracture control	Apathy, immobility, swollen limbs	Inappetence	Trauma	Apathy	Checkup	Checkup	Checkup	Apathy, inappetence

Captive bred = CB, Farm bred = FB, UV index = UVI

\*Varied diets included mostly: mice, rats, chicken, beef, vegetables, eggs

Animals with severe skeletal pathologies

Radiographs of the six animals that were presented at the Clinical Unit of Diagnostic Imaging were taken with a Kodak DirectView PQ storage phosphor screen/cassette system (Carestream, Health Inc., Rochester, NY, USA, 70 kV and 6 mAs) at the University of Veterinary Medicine in Vienna. All radiographs were dorsoventral (vertical beam) and laterolateral (horizontal beam) whole-body images obtained with the animals being placed on a block or in a box without further restraint on the cassette. The radiographs of the animals ID 6, 7, 8 and 9 which were sent in by external veterinarians in DICOM format were all dorsoventral (vertical beam) whole-body images. There was no further information available on the system and modalities used. For CT scans, which were all obtained at the Clinical Unit of Diagnostic Imaging, all animals were comforted awake in plastic boxes without further restraint as well. CT scans were performed with a multi-slice helical CT (Siemens Somatom Emotion, Munich, Germany) using 80 mAs, 130 kV, rotation time 1.5 s, pitch 0.8 and slice thickness 0.75 mm. The scans were reformatted with an ultrasharp bone kernel and a soft tissue kernel, FOV 55 x 55 mm, matrix

size 512 x 512, increment 0.6 mm and then evaluated in a bony and soft tissue window, respectively. All CT scans and radiographs were evaluated with JIVEX, Version 5.3.0.2 RC01 (Visus Health IT GmbH, Bochum, Germany).

The following features were described on radiographs and CT images: overall bone density and exact localization of pathologic changes on any affected bone/joint; presence, extent, shape, subjective density and relation to the compacta of periosteal reactions; involvement of cortical bone, medullary bone changes (density, narrowing) and long bone diameter. The severity of pathologic changes were summarized and documented as well as progression or regression of skeletal pathologies over the period under observation.

Further more density of cortical and medullary bone of humeri, femora and vertebral body of the ninth vertebra, namely the first thoracic/truncal vertebra as well as of the cortical bone and diploe of the os frontale were measured in Hounsfield units (HU) in CT. The first thoracic/truncal vertebra was chosen for comparative evaluation because it is the first of the 17 in size and structure quite uniform vertebrae of the thoracico-lumbar region (Reese 1923) and was therefor deemed representative as a model vertebra. Densitometry of cortical and medullary bone of the appendicular skeleton was performed at three points on cross-section images at the level of the mid diaphysis. For densitometry of the vertebral bodies and the os frontale, corresponding measurements were also taken at three points on cross-sectional images. The vertebral bone density was measured in the middle of the vertebral body. The densitometry of the os frontale was performed in the thickest area of the bone. Maximum, minimum and mean HU were identified using a circular region of interest (ROI) of 0.07 mm<sup>2</sup> to 89 mm<sup>2</sup> depending on the size of the area of interest. In the case of animals ID 1, 2, 3, 4, 5 and 10 where both radiographs and CT images were recorded, the latter were preferred to assess skeletal changes in detail while radiographs served as an overview imaging tool.

In addition to the available imaging recordings, blood chemistry values (ionized calcium, total calcium, phosphorus, total Ca : P ratio, uric acid, total protein, ALP, AST, ALT, CK, GLDH, LDH and bile acid), if available, were evaluated in relation with the clinical findings.



### 3. General results

Of the ten animals, radiographs of all animals and CT images of six animals (ID 1, 2, 3, 4, 5, 10), all of whom were presented at the university facility, were available as is documented in table 2. Six out of ten animals presented with skeletal pathologies detectable by diagnostic imaging, two of which were of traumatic nature (ID 2 – healed old femoral fracture, ID 5 – multiple fractures after a downfall). ID 4 had an extraordinary well mineralized skeleton in which especially the vertebrae appeared similar to a dog or cat suffering from osteopetrosis, displaying overall uniform increased bone opacity with near complete loss of internal cortical margins and medullary cavities in the spine, skull and ribs. Otherwise it appeared normal. Tegu ID 10 showed meniscal mineralizations but was otherwise unremarkable as well. However, two specimens (ID 1 and ID 3) showed massive changes of the long bones of all four limbs, the ribs and the spine. CT scans of these six animals were performed either at initial presentation or during follow-up examinations. Three animals (ID 1, ID 3, ID 5) were presented at the clinic more than once, which allowed to monitor the development of the changes retrospectively. An overview of the available images and findings is given in table 2.

Tab. 2. Diagnostic imaging methods, presence of abnormal radiographic findings, type of radiographic pathology at initial presentation and carried out follow-up examinations

ID	1	2	3	4	5	6	7	8	9	10
Radiography	yes	yes	yes	yes	yes	yes	yes	yes	yes	yes
CT-Scan	no	yes	yes	yes	yes	no	no	no	no	yes
Abnormal radiographic findings	yes	yes	yes	yes	yes	no	no	no	no	yes
Type of radiographic pathology	bilateral soft tissue mass near last ribs	old femur fracture	severe bone deformation and destruction	increased density of vertebrae and skull	multiple fractures	-	-	-	-	slightly increased density of vertebrae, mineralized menisci
Follow-up examination (number of follow-up examinations)	yes CT (2), Rx (2)	no -	yes CT (1), Rx (1)	no -	yes Rx (3)	no -	no -	no -	no -	no -

#### Animals with severe skeletal pathologies

Animal ID 2, apart from the traumatic healed fracture, was clinically and radiographically unremarkable. Due to its proper husbandry and its well known optimal nutritional conditions it was used as a healthy and normal comparison animal for specimens ID 1 and 3 that were suffering from massive skeletal pathologies (Fig. 1). The other seven radiologically MBD-unaffected animals (ID 4, 5, 6, 7, 8, 9 and 10) were used for comparison additionally.

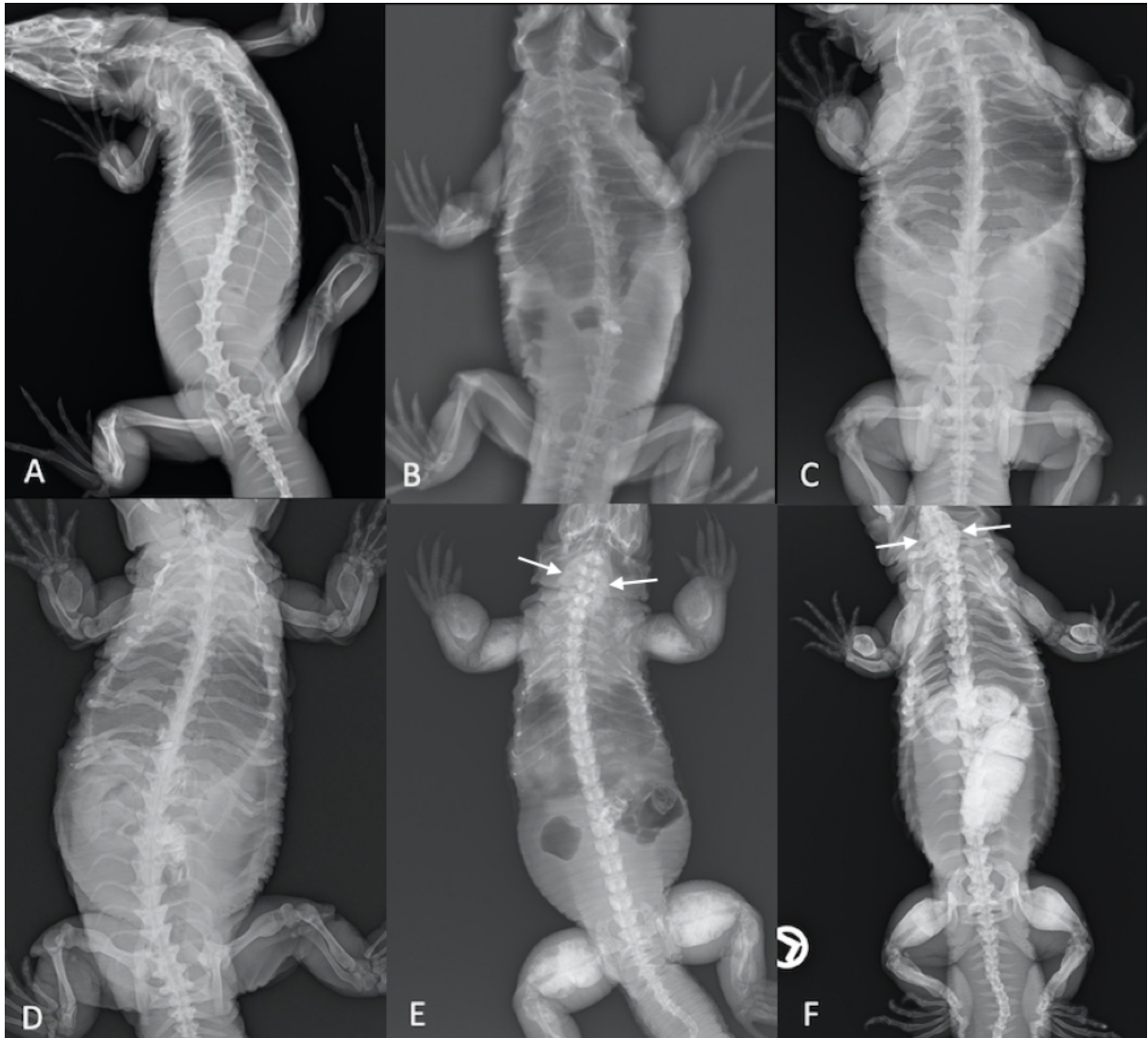


Fig. 1. Comparative dorsoventral radiographs of three different tegus. **A** represents the normal reference animal (ID 2) with well mineralized slim long bones without any periosteal new bone formations. **B**, **C** and **D** represent tegu ID 1 from 13.6.2016, 15.1.2018 and 15.6.2020, respectively, while **E** and **F** are tegu ID 3 from 14.12.2017 and 5.11.2019. The bony changes are described in detail in the individual case reports. It is remarkable that the changes of the cervical spine in tegu ID 3 (white arrows) are also seen on these dorsoventral radiographs.

The densitometric results as well as the blood chemistry values of six of the animals (ID 1, 2, 3, 4, 5, 10) from at least one or more examination included in this study are listed in table 3 and 4. An interesting finding of this study was that in the clinically and radiographically not MBD affected tegus, regardless of sex and age, cortical bone density was quite high and even animal ID 1 displayed an unusually high bone density at the second follow-up examination.

Due to the alike clinical presentation in animals ID 1 and 3 at the time of onset of clinical symptoms, similar massive radiographic changes visible at that time in both animals and the manifold diagnostic imaging documentation, these two cases are hereby presented in further detail.

Tab. 3. Mean ( $\pm$  SD) and range of bone mineral density of six specimens

ID	1			2	3		4	5	10
Age at presentation	1y 1m	2y 5m	4y 10m	1y 11m	1y 11m	3y 10m	4y	1y	8y
Weight (g)	1058	1900	unknown	1745	848	1855	7620	1170	7000
<b>BMD of cortical bone left humerus (HU)</b>									
MV ( $\pm$ SD)	719 (44)	612 (118)	947 (98)	1868 (102)	419 (30)	1084 (13)	1840 (231)	1813 (124)	1722 (155)
Range	664-771	472-760 (x)	815-1050	1761-2006	379-450 (o)	1070-1102 (xxx)	1552-2118	1653-1955	1517-1890
<b>BMD of cortical bone right humerus (HU)</b>									
MV ( $\pm$ SD)	722 (84)	786 (59)	951 (115)	1733 (87)	454 (22)	922 (65)	1850 (138)	1773 (229)	1683 (112)
Range	607-802	712-857 (xx)	806-1088	1612-1811	426-479 (o)	841-1001 (xxx)	1740-2045	1471-2025	1533-1803
<b>BMD of cortical bone left femur (HU)</b>									
MV ( $\pm$ SD)	802 (46)	1112 (95)	1522 (100)	1697 (306)	402 (11)	1147 (45)	2013 (134)	1698 (275)	1622 (22)
Range	743-855	1011-1240	1381-1596	1301-2047	389-416 (o)	1085-1191 (xxx)	1839-2165	1341-2009	1316-1846
<b>BMD of cortical bone right femur (HU)</b>									
MV ( $\pm$ SD)	782 (87)	987 (46)	1556 (64)	1695 (100)	469 (20)	979 (38)	1991 (43)	1891 (164)	1758 (240)
Range	671-884	940-1049	1485-1640	1563-1805	445-495 (o)	938-1029 (xxx)	1937-2043	1672-2066	1432-2001
<b>BMD of cortical bone vertebral body (9th vertebra)</b>									
MV ( $\pm$ SD)	600 (44)	898 (58)	1011 (40)	1465 (43)	705 (50)	1051 (0)	1769 (222)	1535 (99)	1511 (102)
Range	554-660	854-980	963-1061 (x)	1404-1500	639-761 (xx)	1051-1051 (x)	1485-2028	1396-1623	1380-1628
<b>BMD of cortical bone os frontale (HU)</b>									
MV ( $\pm$ SD)	469 (19)	601 (58)	871 (40)	1320 (144)	351 (41)	1528 (96)	1765 (171)	1701 (31)	1610 (218)
Range	443-486	533-675	843-909	1118-1445	311-407	1396-1623	1612-2003	1669-1742	1344-1879
<b>BMD of medullary bone left humerus (HU)</b>									
MV ( $\pm$ SD)	157 (230)	521 (136)	233 (256)	57 (143)	172 (66)	324 (414)	268 (829)	456 (0)	165 (91)
Range	-73-386	385-656 (x)	-23-488	-86-200	106-238	-90-737 (xxx)	-561-1097	456-456	74-255
<b>BMD of medullary bone right humerus (HU)</b>									
MV ( $\pm$ SD)	169 (136)	557 (139)	280 (288)	55 (78)	153 (124)	312 (309)	376 (515)	161 (150)	288 (162)
Range	33-304	418-695 (xx)	-8-567	-23-132	29-277	3-621 (xxx)	-139/891	11-310	126-450
<b>BMD of medullary bone left femur (HU)</b>									
MV ( $\pm$ SD)	260 (301)	543 (99)	410 (444)	-70 (63)	75 (54)	435 (533)	-68 (506)	42 (114)	79 (98)
Range	-41-560	444-642	-34-853	-133- -7	21-128	-98-968 (xxx)	-574-438	-72-155	-19-177
<b>BMD of medullary bone right femur (HU)</b>									
MV ( $\pm$ SD)	324 (267)	534 (119)	368 (306)	119 (247)	56 (63)	421 (500)	56 (306)	62 (104)	61 (61)
Range	57-590	415-652	62-674	-128-366	-7-119	-79-920 (xxx)	-250-362	-42-166	0-121
<b>BMD of medullary bone vertebral body (9th vertebra)</b>									
MV ( $\pm$ SD)	374 (12)	686 (61)	734 (111)	518 (210)	401 (82)	1060 (42)	828 (131)	650 (94)	870 (248)
Range	362-385	625-746	623-844 (x)	308-728	319-482 (xx)	1018-1101 (x)	697-959	556-744	622-1117
<b>BMD of medullary bone os frontale (HU)</b>									
MV ( $\pm$ SD)	427 (55)	561 (102)	604 (123)	348 (393)	191 (141)	995 (288)	346 (770)	499 (307)	648 (600)
Range	372-481	459-662	481-727	-45-741	50-332	707-1282	-424-1116	192-805	48-1248

**Animals with severe skeletal pathologies**

BMD = bone mineral density; HU = Hounsfield units, MV = mean value, SD = standard deviation

(x) no distinction between cortical bone and medullary bone possible (measurement where cortical/medullary bone was suspected if possible)

(xx) partly distinction between cortical bone and medullary bone possible

(xxx) distinction between cortical bone and medullary bone difficult in area of new bone formation

(o) distinction between cortical bone and periosteal reaction hardly possible



Tab. 4. Blood chemistry values of six specimens

ID	1			2	3			4	5	10
Age at presentation	9m	1y 1m	2y 5m	1y 11m	1y 11m	2y		4y	1y	8y
Weight (g)	1058	1086	1900	1745	848	848	unknown	7620	1170	7000
Ionized calcium (mmol/L) (1.0 ± 0.49)** (mg/dL) (4.0 ± 1.97)**	-	0.66	1.05	-	0.64	1.08	0.77	-	-	-
	-	2.65	4.21	-	2.56	4.33	3.09	-	-	-
Total calcium (mmol/L) (3.04 ± 0.2)* (mg/dL) (12.2 ± 0.8)*	1.86	2.96	2.42	2.67	1.54	2.33	2.24	3.1	2.47	2.56
	7.45	11.86	9.7	10.7	6.17	9.34	8.98	12.42	9.9	10.26
Phosphorus (mmol/L) (1.8 ± 0.68)* (mg/dL) (5.6 ± 2.1)*	0.75	1.23	1.78	1.17	1.63	1.33	1.32	1.34	1.22	1.45
	2.33	3.81	5.52	3.63	5.05	4.12	4.09	4.15	3.78	4.5
Total calcium : Phosphorus ratio	2.5	2.4	1.4	2.3	0.9	1.8	1.7	2.39	2.0	1.7
Uric acid (mg/dL) (0.5-13.2)***	0.5	1.6	1.2	2.8	0.8	1.2	1.5	-	1.5	-
Total protein (g/dL) (4.0-8.3)***	-	5.39	5.06	5.7	4.6	4.1	-	-	4.21	-
ALP (U/L) (160 ± 85)*	-	77	100	-	-	-	-	-	-	-
AST (U/L) (18 ± 14)*	12	12	7	20	-	-	-	-	-	-
ALT (U/L) (33 ± 24)*	21	-	11	44	4	-	-	-	-	-
CK (U/L) (641 ± 568)***	4575	685	229	548	589	-	-	-	-	-
GLDH (U/L) (x)	6.51	10.32	1.43	4.55	2.53	-	-	-	-	-
LDH (U/L) (540 ± 537)*	-	-	-	185	155	-	-	-	-	-
Bile acid (μmol/L) (x)	6	18	10	-	-	-	-	-	-	-

Animals with severe skeletal pathologies

(Reference values \*Carpenter 2018, \*\*ZIMS 2021, \*\*\* ZIMS 2022, x no species specific reference values available)

## **4. Case report A – animal ID 1**

### **4.1. Animal data, medical history**

A nine months old subadult black and white tegu (*Tupinambis merianae*) was initially presented to the department for birds and reptiles of the small animal hospital of the University of Veterinary Medicine Vienna in May 2016 because of two palpable subcutaneous rounded, solid masses located bilaterally in the region of the last ribs. The animal was kept solitary in an enclosure with an UV high intensity discharge (HID) lamp which had been renewed approximately four months ago. No information on the brand, type or wattage/UV index of the lamp or the daily exposure time was available. The animal's diet consisted mainly of fuzzy mice without further (mineral) supplementation every two days. Additionally, it was fed raw chicken, beef and pork meat without supplementation once a week.

### **4.2. Clinical examination**

During the physical examination the animal presented in good general condition, displaying active behavior and an age-appropriate weight of 1058g. On palpation of the suspected masses it was not clear if they were expanding into the coelom. They were not painful on palpation, not movable, had a solid consistency and measured about 2 x 2 cm. Otherwise the animal was clinically unremarkable.

### **4.3. Diagnostic imaging**

For further diagnostics a whole-body radiograph was performed. The palpable masses, measuring about 2 cm in diameter on the left and about 2.4 cm on the right side, were only partially demarcated, mostly homogenously soft tissue dense and located subcutaneously. A connection to both last ribs could not be definitely ruled out. As a secondary finding, a spindle-shaped smooth bone swelling was noted in the mid diaphysis of the right ulna, which was diagnosed as an old, healed fracture. The rest of the skeleton was radiologically quite well mineralized and unremarkable at that time. Additionally to the radiograph, an ultrasound examination was then performed, in which the masses were diagnosed as subcutaneously located, solid tissue spreading around the ribs with heterogenous echogenicity and a well-defined margin. The ribs embedded in the mass could be clearly differentiated and no



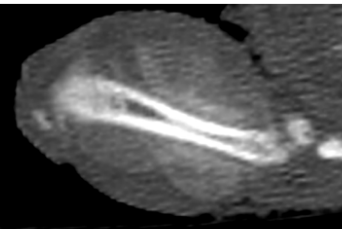
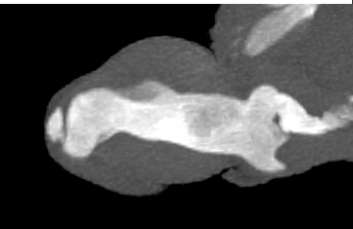
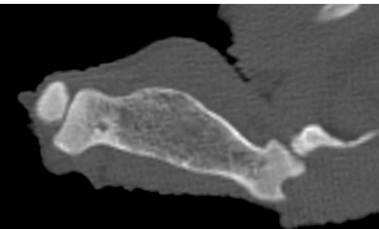
infiltration by the masses was detectable. The suspected diagnosis was granuloma formation with neoplasia as less likely differential diagnosis.

To obtain a definite diagnosis a fine needle aspiration biopsy was suggested to the owner, but not performed as he did not deem it necessary at that time.

#### **4.4. Therapy, course of disease**

A consultation about necessary housing (installing a new UV-B HID lamp) and dietary (more varied diet of vegetables, whole prey items, fruits and insects with calcium supplementation) changes was conducted and a follow-up examination scheduled. From the initial presentation in May 2016 until June 2020 the animal was presented to the clinic a total of five times due to various reasons, either for follow-up examination or medical support. Each time either radiographs (Fig. 1 B, C and D) or CT scans were performed. In table 5 the reason for each presentation, result of physical examination, type of performed diagnostic imaging, main localization of skeletal changes, density of affected areas in HU, important additional information and if available total calcium, ionized calcium and phosphorus are listed.

Tab. 5. Overview of clinical and diagnostic imaging history of animal ID 1

Date of presentation	May 2016	June 2016	October 2016	January 2018	June 2020
Reason for presentation	local swellings	GIT prolapse	front limb swelling	follow-up examination	follow-up examination
Physical examination	bilateral solid masses adjacent to ribs	cloacal prolapse due to foreign body	massive front leg soft tissue swelling, known masses less marginated than before, tremor in both front legs	forelimb swellings same size as last time, additional approx. 6 x 4 x 15mm sized swelling on both hind limbs, slight hind leg muscle atrophy, movement slightly impaired (inadequate lifting of the trunk when moving forward)	unremarkable, no changes to last examination
Total calcium (mmol/L) (3.04 ± 0.2)* (mg/dL) (12.2 ± 0.8)*	not evaluated	1.86 7.45	2.96 11.86	2.42 9.70	not evaluated
Ionized calcium (mmol/L) (1.0 ± 0.49)** (mg/dL) (4.0 ± 1.97)**	not evaluated	not evaluated	0.66 2.65	1.05 4.21	not evaluated
Phosphorus (mmol/L) (1.8 ± 0.68)* (mg/dL) (5.6 ± 2.1)*	not evaluated	0.75 2.33	1.23 3.81	1.78 5.52	not evaluated
Performed diagnostic imaging	radiography	radiography	radiography, CT	radiography, CT	CT
RX / CT main locations	right ulna, ribs	expansion of known rib adjacent masses	ribs, both humeri, radii, tail; ulnae not changed	humeri, radii, ulnae, femora, right tibia, ribs	humeri, radii, ulnae, femora, right tibia, ribs
Figure (right humerus)					
Figure type	radiography	radiography	CT bony window	CT bony window	CT bony window
Densitometry	-	-	masses adjacent to long bones: up to 135 HU masses adjacent to ribs: 58-160 HU	masses adjacent to long bones: up to 565 HU cortical bone of long bones: up to 1240 HU	cortical bone of long bones: up to 1640 HU
Additional information	-	improved diet and husbandry	samples taken for bacteriology and histopathology	improved diet and husbandry	-
Further findings	-	-	histopathology: newly formed, regular bone tissue, bacteriology was negative	distinction between original bone and new bone tissue formation not possible	formations have smoothed and organized, distinction between cortical and medullary bone is possible again

(Reference values \*Carpenter 2018, \*\*ZIMS 2021)



When the animal was presented again in June 2016, shortly before the scheduled follow-up examination, this time because of a cloacal prolapse and gastrointestinal (GIT) foreign body, both the performed radiograph and the ultrasonography revealed a slight growth of both known masses.

In October 2016, the animal was presented with massive swelling of both front limbs which is most often seen with fibrous osteodystrophy due to NSHP, bone neoplasia, hypertrophic osteopathy, traumatic fractures or osteomyelitis. On radiographs and CT images severe changes around the diaphysis and metaphysis of the humeri and radii, but only minor changes around the ulnae were visible. The swollen areas presented as symmetrical, smoothly bordered, slightly cloudy soft tissue swellings with soft tissue opacity and focal changes similar to the ones adjacent to the ribs with higher opacities up to 135 HU. The altered tissue was not visibly connected to the bones, but was directly adjacent to them around the diaphysis and metaphysis and could be connected to the periosteum. Around the ulnae, slight, symmetrical soft tissue swellings with distinct margins and densities that were partly similar to the ones around the ribs were visible.

The density of the cortical bone was reduced in both humeri and femora (max. 884 HU) as well as the cortical density of the os frontale (max. 479 HU) compared to literature references (1000 HU) (Pees 2010b) and the main control animal ID 2 (Median BMDs of left humerus 1836 HU, right humerus 1775 HU, left femur 1742 HU, right femur 1716 HU, os frontale 1283 HU). Due to the smoothly delineated, presumably periosteal reactions, the intactness of the cortices and the distinct transition zones of the lesions, non-aggressive metabolic bone lesions were suspected. No pathologic fractures were visible.

The masses adjacent to the last ribs presented massively enlarged compared to the last radiographic images, especially ventrally to the ribs (approx. 4.9 x 2.2 cm on the left and ca 4.3 x 2.5 cm on the right side), and cloudy with heterogenous opacity (58-160 HU), which is above the normal mean density of soft tissue in reptiles (40-50 HU) (Gumpenberger 2011). Compared to the previous images, this time smoothly delimited, <1 mm high periosteal reactions of homogenous density as well as lysis of the adjacent or surrounded ribs could be observed. The massive expansion of the masses visibly led to a significant compression of the lungs, with a significant deformation of the caudal lung contours. None of the visible changes, neither the ones affecting the front legs nor the ones affecting the ribs, showed any joint involvement.

There was also no evidence of involvement of the distal extremities (toes), which were not visibly affected in any way. In the vertebral bodies a generalized higher density was apparent. With regard to the progressive expansion of the rib-associated masses, a neoplastic event was deemed unlikely at that time due to the multifocal and generally symmetrical appearance of the pathological changes, but could still not be entirely ruled out based solely on the radiographic findings. For further investigation and to obtain a clearer diagnosis, a sample of one of the rib-adjacent masses was surgically removed according to clinic standards under general and local anesthesia. For general anesthesia 0.15 mg/kg medetomidine i.m. and 0.5 mg/kg morphine i.m. were used for premedication, alfaxalone 2 mg/kg i.v. for induction, then the animal was intubated and maintained with isoflurane and manual ventilation in dorsal recumbency. An intercostal nerve block with 3 mg/kg ropivacaine was used for local anesthesia of the surgical site on the left thoracic wall right above the palpable mass. During surgery the mass appeared macroscopically solid, slightly adjacent to the surrounding tissue and located between the penultimate and last rib. Immediately after surgery the animal received 0.2 mg/kg meloxicam i.m. and on the same afternoon 0.3 mg/kg morphine i.m. for additional post-surgery analgesia. After the animal had recovered from surgery the following day it was discharged from the clinic with meloxicam (0.2 mg/kg) for the next 7 days. The owner was also advised to switch to feeding older mice instead of fuzzy mice because of their higher Ca : P ratio, to stop supplementing Vitamin D3 which he offered twice a week and instead to add proper pure Ca supplementation in form of commercially available calcium products in the product-specific recommended dosage and to install a new UV-B HID lamp (no detailed information was documented in the patients documents).

The result of the bacteriological examination of the sample was negative. The histological examination at the institute of pathology of the University of Veterinary Medicine Vienna revealed that the obtained sample consisted of multiple bone trabeculae surrounded by osteoblasts and of fibrovascular stroma with numerous multinucleated giant cells (osteoclasts). As the regular structure and the even arrangement of the trabeculae with surrounding osteoblasts were typical for a reactive new bone formation and excluded a neoplastic genesis, the diagnosis “newly formed, regular bone tissue” was made.

In January 2018, the animal was again presented for a radiography and CT follow-up examination and corresponding blood chemistry (see table 4). Clinically the animal was active and alert but displayed slightly impaired movement (not lifting its' trunk off the ground when walking) and mild hind limb muscle atrophy as well as bilateral, solid, not painful swellings of the femora. When evaluating the radiographs and CT images, it was immediately evident that the changes had undergone a massive progression since the last images had been taken as both humeri and radii displayed severe deformations (Fig. 2, B).

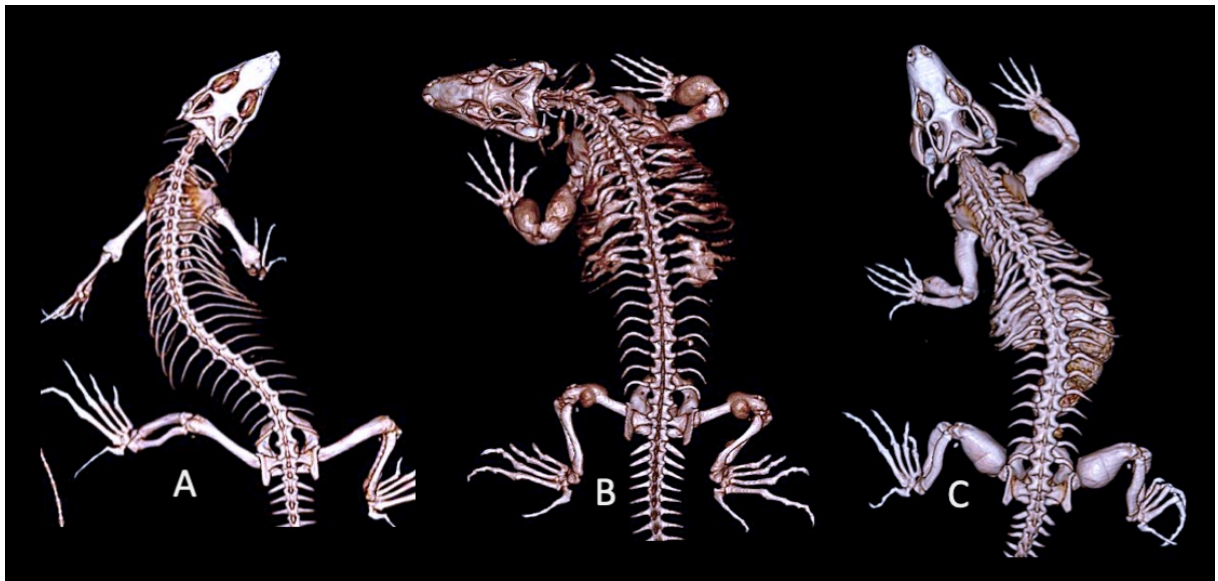


Fig. 2: Comparative 3D CT reconstruction of the skeleton in three tegus. **A** is the reference tegu ID 2, **B** is tegu ID 1 from 15.01.2018 and **C** is tegu ID 3 from 05.11.2019. In **B** the massive, bullous changes of the humeri and radii are clearly visible as well as the new formations affecting both femora of animal ID 1. **C** is from a follow-up examination of animal ID 3 with pronounced re-organized and smoothed long bones. Note the extensive alterations of the ribs in both **B** and **C**.

A bullous swelling of the bone with up to three times the diameter of the original bone extended over the entire diaphysis of the left humerus. The medullary cavity could not be identified except for a small area in the distal diaphysis, so distinction between a potentially expanded compacta and a potentially ossified medullary space was impossible. The previously hyperdense soft-tissue adjacent to the bone have further gained density up to 565 HU and have fused with the underlying bone, which no longer allowed distinction between original bone and new bone tissue formation. From this point on it has to be addressed rather as a complete increase in bone circumference than as a periosteal reaction. The right humerus presented with similar bullous alterations and swelling up to twice its diameter in some localizations (Fig. 3,

A). Although the medullary cavity showed a generally higher opacity as well, it could still be clearly defined over parts of the diaphysis. Here too, the formerly hyperdense soft-tissue has condensed to 532 HU and fused with the underlying bone. With exception of the epiphyses and partly metaphysis, both radii had a bullous appearance as well, with diameters up to 15.5 mm or 17 mm and showed the same fusions of previous new hyperdense tissue and original bone with densities up to 536 HU in the altered areas. Both radii showed generalized highly condensed medullary cavities and it was not possible to distinguish between ossified medullary canal or expanded compacta. Both ulnae displayed much less pronounced changes of similar characteristics than the humeri and radii. Still, there were no periosteal reactions or other pathologic changes detectable in the metacarpal region and the digits.

In addition to the already familiar changes in the forelimbs, now similar bilateral changes presented in the hind limbs (Fig. 3, B). While the left tibia appeared normal, the right tibia showed comparable moderate to severe changes to those of the femora in the distal diaphysis, with periosteal reactions up to 3.5 mm height and with density up to 400 HU. The medullary cavity appeared generally compressed. Both fibulae and the metatarsal bones as well as the digits were unaffected. Similar to the last radiographic findings, the changes in all long bones were limited to the diaphysis and, in some cases, also the metaphysis of the bones, but no joint involvement could be detected. All formations appeared smoothly demarginated and of relatively homogeneous density, so that it can be assumed that there were no reactive areas at this point.

The already familiar changes affecting the ribs had highly progressed further at this time. All ribs displayed a generalized expansion and deformation with up to 2-3 times increase in diameter. Bilaterally several ribs were fused together by bone-dense structures so that no differentiation between ribs and the newly formed bone material was possible any more (Fig. 1, C). The fused areas were mostly homogeneous bone-dense with small lytic areas. The medullary cavities of the affected ribs could only be identified in some areas. In all ribs, solid, smoothly demarginated, relatively homogeneous bone-dense periosteal reactions up to 2 mm height were visible. However, the masses compressing the lungs at the last radiographic examination had almost disappeared. The spine displayed a generalized increased density (up to 980 HU) of all vertebrae and therefore, the medullary cavity could no longer be clearly

distinguished. Overall, the entire skeleton subjectively appeared to have an increased density compared to the last images.

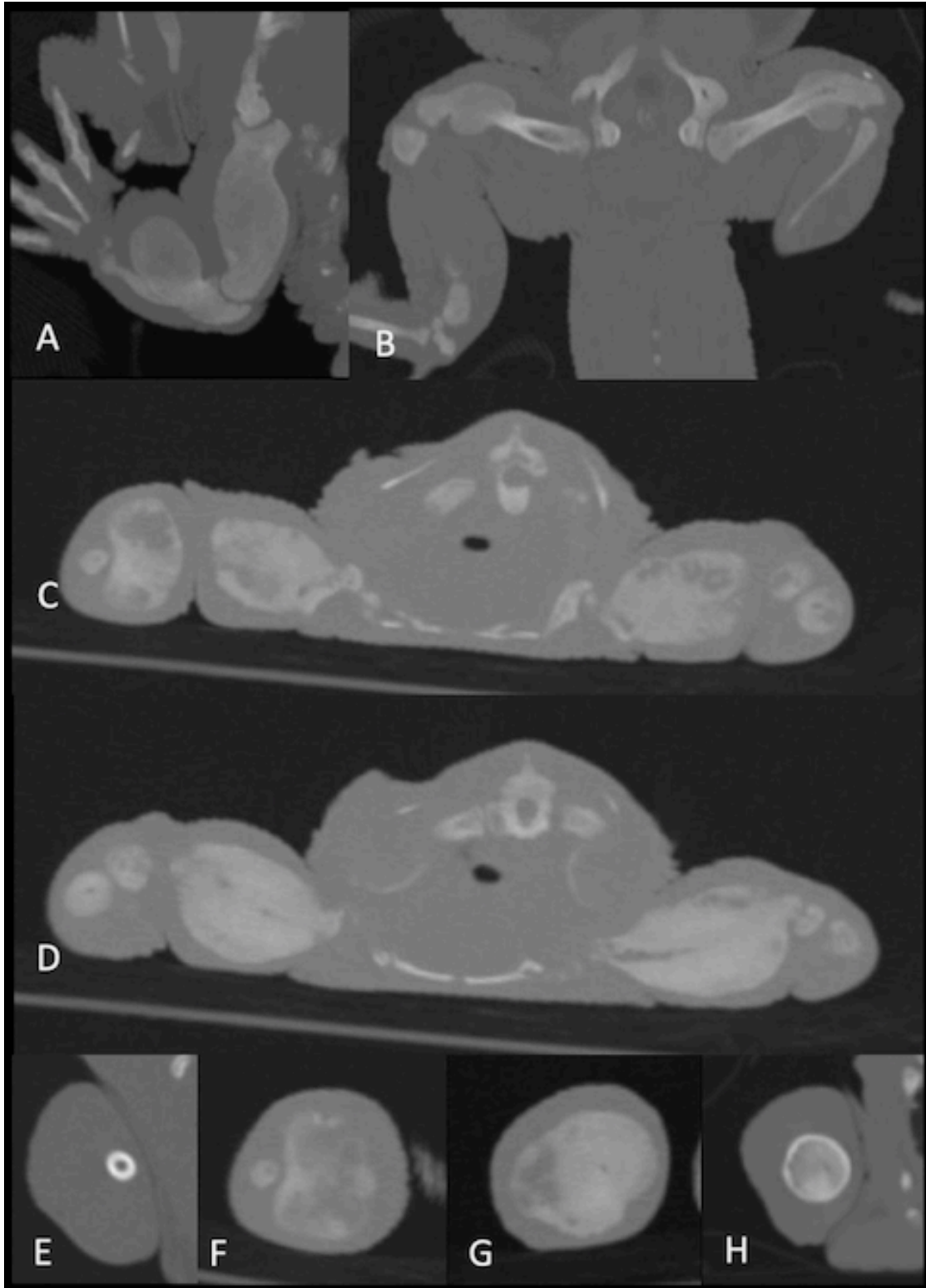


Fig. 3. Comparative multiplanar reconstructions of CTs in bony window of three different tegus, **A** (left front limb) and **B** (both hind limbs) coronal plane, **C** and **D** (both front legs) transverse (body) /sagittal (humerus) plane aligned to fit the body region shown, **E** to **H** transverse plane of the left humerus. **A** and **B** represent tegu ID 1, **C**, **D**, **F**, **G** and **H** represent tegu ID 3 (**C**, **D**, **F** and **G** from 14.12.2017 and **H** from 5.11.2019) and **E** is the normal reference animal ID 2. Note the bullous alterations and swelling of the right humerus with up to twice its original diameter extending over the entire diaphysis in **A** with a generalized hyperdense medullary cavity which makes it nearly impossible to distinguish between a seemingly expanded cortical or maybe ossified medullary bone in most areas. In **B** there are similar bilateral changes visible in the femora, which display bullous swelling that enclose the bones in the area of the distal diaphysis. The cortical bone appears intact and displays no changes, while up to 5mm high and solid (left leg) and 6mm high and cloudy (right leg), smoothly demarginated, relatively homogeneously bone-dense periosteal reactions with densities up to 400 HU were discovered. The medullary cavity presented irregularly compacted. In **C** and **D** both humeri display massive cloudy smoothly demarginated swellings of presumably periosteal origin with heterogenous density of about three times the bone diameter. Medullary cavities are partly indistinguishable from the compacta. In **F** and **G** the cloudy, heterogenous, but mostly smoothly demarginated appearance of the changes of the left humerus of animal ID 3 is clearly visible. In **H** the bony alterations are now visibly condensed and smoothed. It is not clearly distinguishable what is massively narrowed, respectively mostly ossified medullary cavity or expanded compacta although the highly hyperdense, thin outline of the bone may represent the compacta. In comparison a clear distinction between hypodense medullary cavity, hyperdense cortical bone and surrounding soft tissue is possible in **E**.

Further new findings were bilateral changes in the cranial ilium, which showed expansive growth in the same manner as the humeri. Differential diagnoses at this point were MBD, multilobular osteochondroma or neoplasia of another genesis. Unfortunately, the owner declined taking any samples. Most likely, because the animal was clinically so far in a good general condition, and was therefore sent home with the advice to return in case of deterioration of general condition, locomotion difficulties and/or further progression of the limb swelling. According to the owner the animal's diet at that time consisted of raw chicken meat and beef with mangos, champignons, apples, paprika, boiled eggs and cooked vegetables (beans, corn) every second day and sometimes fuzzy mice and was supplemented with Calcium and Vitamin D3 once a week. He had also installed a new UV-B HID lamp four months ago. However, the owner was unable to name the brand of the lamp or provide more detailed information about the mineral and vitamin supplementation.

The animal was last presented in June 2020 for a follow-up examination. No abnormalities were reported by the owner and the physical examination was inconspicuous. On the radiographs and CT images it was clearly evident that all known formations affecting the long bones were now smoothly organized (see Fig. 1, D). The compacta could be identified in all bones, the medullary cavities were mostly visible and only displayed increased density in some areas. The previous new bone formations adjacent to the humeri and radii measured now up to 14/12.7

mm in height. The changes affecting the ribs with fusion of numerous ribs were still massive, but also a little more smoothed and organized. The vertebral medullary cavities were still highly hyperdense, even more than at the last examination (up to 1061 HU), and could not be differentiated from the compacta. No Blood samples were taken. At that time the animal was mainly kept outdoor on the balcony with direct access to natural sunlight most of the year. Therefor the owner only used a UV-B HID lamp during the winter when the animal was kept inside. The owner had reduced the feeding frequency and increased the percentage of different vegetables and fruits in the tegu's diet. For supplementation pure calcium was used. Unfortunately, the owner didn't provide more detailed information about the used calcium product (brand, frequency of supplementation, quantity used) or the exact composition of the tegu's diet.

To the current day, the animal is doing clinically well.

## 5. Case report B – animal ID 3

### 5.1. Animal data, medical history

In December 2017, a subadult black and white tegu, which had been confiscated by the authorities for violation of animal welfare, was presented to the Department for Birds and Reptiles of the Small Animal Clinic of the Vetmeduni Vienna. According to information passed on to the clinic the animal was one year and eleven months old but there were no corresponding documents recorded. The animal was presented in a poor general condition due to apathy and massive swelling on all four extremities. Before the confiscation, the animal had been kept ranging free in an apartment together with an older conspecific. Its diet consisted exclusively of fuzzy mice according to available recordings and no information was available on supplementation or access to UV-B light.

### 5.2. Clinical examination, laboratory diagnostics

The animal was apparently too small for its presumed age (848 g, Köhler and Langerwerf, 2000). During the physical examination, massive, painful swellings of all four extremities, around the ribs and the tail base were noted (Fig. 4) as well as tremor in the hind limbs. The tegu's body condition was poor, the general condition was slightly reduced. Furthermore, several teeth were missing and the animal displayed a disability to lift its body off the ground for locomotion.



Figure 4. Subadult *Tupinambis merianae* (ID 3) with pronounced swelling of all four limbs



Hematology (Tab. 6) and blood chemistry were done the same day. Blood chemistry showed total calcium of 1.54 mmol/l (6.17 mg/dL), phosphorus of 1.63 mmol/L (5.05 mg/dL), which is an inverse Ca : P ratio of 0.9:1 and ionized calcium of 0.64 mmol/l (2.56 mg/dL). Overall, a severe hypocalcemia was diagnosed based on the available reference values for total calcium ( $3.04 \pm 0.2$  mmol/L) and phosphorus ( $1.8 \pm 0.68$  mmol/L) (Carpenter 2018) and ionized calcium ( $1.0 \pm 0.49$  mmol/L) (ZIMS 2021). All blood chemistry values are listed in table 4.

Tab. 6. Hematology of animal ID 3 at initial presentation

Hematocrit (%) ( $25 \pm 2.3$ )*	31
WBC / 400 HPF ( $16.65 \pm 2.24$ )*	13
Lymphocytes (%) ( $45.6 \pm 6.8$ )*	11
Monocytes (%) ( $6.5 \pm 1.4$ )*	6
Azurophils (%) ( $11.5 \pm 3.2$ )*	-
Heterophils (%) ( $12.1 \pm 2.12$ )*	74
Eosinophils (%) ( $25 \pm 3.4$ )*	-
Basophils (%) ( $2 \pm 0.8$ )*	9

White blood cells = WBC, High power field = HPF

(Reference values for female *Tupinambis merianae* \*Troiano et al 2008)

### 5.3. Diagnostic imaging

On the same day, a dorsoventral whole-body radiograph (Fig. 1, E) and whole-body CT images were taken. The overall bone density was initially deemed normal on the radiographs as the transverse processus of the caudal vertebrae could be distinguished from the surrounding soft tissue. On the other hand the digits' density appeared massively reduced. In the subsequent CT the cortical bone density of the os frontale (max. 407 HU) as well as the femora (left femur

max. 416 HU, right femur max. 495 HU) and humeri (left humerus max. 450 HU, right humerus max. 479 HU) was also found to be significantly reduced.

On radiographs and CT images alike, both humeri showed massive cloudy, smoothly demarginated swellings of presumably periosteal origin with heterogeneous density (bone-dense areas with 390 HU to soft-tissue areas with 69 HU) with about three times the bone diameter. The medullary cavities were partly indistinguishable from the compacta and partly clearly visible (Fig. 3, C, D, F, G). The radii were both generalized massively changed, whereby neither the medullary cavities nor the compacta could be identified and the original bone could no longer be differentiated from the surrounding masses and reactions. The presumed new formations were up to 15.6 mm and 17 mm high and 20.6 mm and 14 mm wide, cloudy, smoothly demarginated and of heterogeneous density (bone-dense areas with 419 HU to soft-tissue areas with 45 HU, similar to moth-eaten osteolysis). The distal end of the left radius could no longer be identified, the distal end of the right radius could only be roughly identified. Compared to the humeri and radii, the changes affecting the ulnae were only slight to moderate with up to 2.8 mm high (same diameter as underlying bone), solid, smoothly demarginated and relatively homogeneous bone-dense (max. 431 HU) periosteal reactions.

Like the humeri, both femora displayed massive changes over the entire diaphysis and parts of the metaphysis with cloudy, smoothly demarginated periosteal reactions of heterogeneous density (64.5 HU up to 373 HU) with up to 4.3 times the diameter of the bone. Periosteus, primarily bone-dense areas were noticeable, while soft-tissue areas with a bone-dense “shell” predominated further in the periphery of the mass. The periosteal reaction on the left femur also had a partially bullous appearance. The medullary cavities of both femora were clearly visible to slightly shaded or partially narrowed and there was a suspected expansion of the compacta. The left tibia showed cloudy, partially bullous-like, smoothly demarginated periosteal reactions of heterogeneous density (80 HU up to 247 HU) on the proximal diaphysis with about the same diameter as the bone and also a suspected generalized expansion of the compacta. The right tibia was slightly to moderately changed at the proximal and distal diaphysis and showed a visible expansion of the compacta. The proximal end of the right tibia could not be identified. The periosteal reactions were about 13 mm long and up to 3.3 mm high (same diameter as underlying bone), solid, smoothly demarginated and of relatively homogeneous bone density (347 HU). The medullary cavities of both tibiae appeared normal. The fibulae were both

changed at the diaphysis, especially proximally, and moderately also at the metaphysis, the compacta being possibly expanded on the left and visibly expanded on the right side. The periosteal reactions were solid, smooth and in some cases of heterogeneous density (146 HU up to 330 HU).

Despite the severity of these radiographic findings, none of the numerous changes of the long bones showed any joint involvement. The distal limbs (metacarpal and metatarsal bones, toes) were also not visibly affected. The ribs were also massively altered with generalized expansion and up to 3.4 mm high, solid, smoothly demarginated, relatively homogeneously bone-dense (up to 371 HU) periosteal reactions. The vertebral bodies showed a generalized opacity of up to 714 HU and the medullary cavity could not be identified. Furthermore, ventral to the osteopetrosis-like dense and fused cervical vertebrae 1-5 a massive, cloudy, heterogeneous (69 HU up to 326 HU) mass with dimensions of about 40 mm x 11 mm x 20 mm was detected (Fig. 5, C, D). The trachea was displaced ventrally by the formation and the cranial lung areas were slightly compressed and deformed as well. The caudal spine displayed multiple scoliosis.

Differential diagnoses at that time included acropachy (hypertrophic osteopathy), hypercalcemia and osteopetrosis, hypervitaminosis A and periostitis. NSHP or renal secondary hyperparathyroidism (RSHP) were not listed as main differentials at first due to the solid and dense nature of the bony changes that were more associated with the typical radiographic signs of acropachy in mammals. The missing teeth noted during the physical examination were confirmed in the radiographic examination.

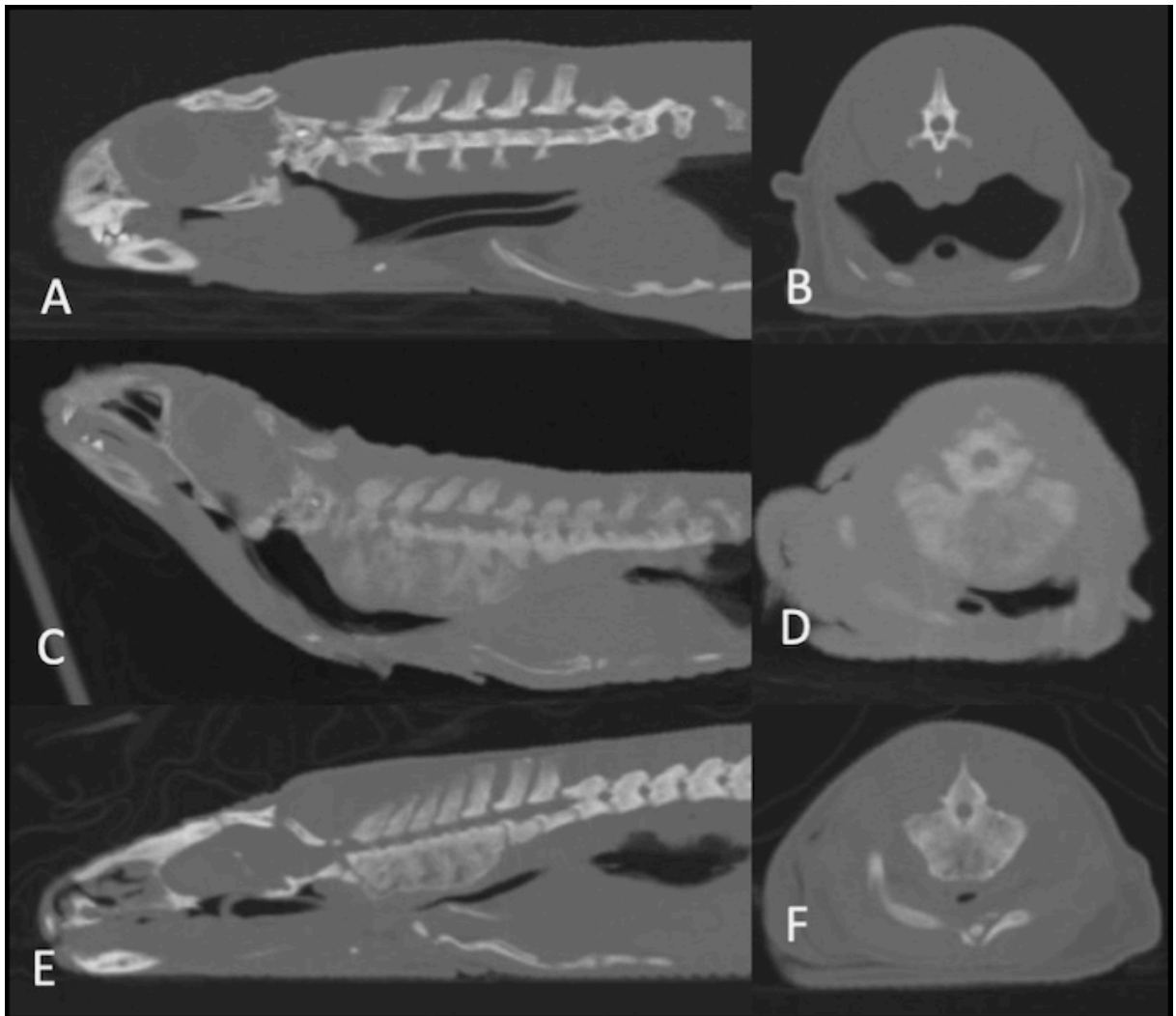


Fig. 5. Comparative multiplanar reconstructions of CTs in bony window of the head and cervical spine of two different tegus, **A**, **C** and **E** in sagittal and **B**, **D** and **F** in transverse plane. **A** and **B** represent tegu ID 2 and **C** to **F** represent tegu ID 3 (**C** and **D** from 14.12.2017 and **E** and **F** from 5.11.2019). There are severe, at first more spongy and later on more solid new bone formations ventral to the cervical vertebrae in the affected animal ID 3. Note the overall reduced bone density of the diseased animal (ID 3) in comparison to the healthy animal (**A** and **B**). However, the density improved from 2017 to 2019.

#### 5.4. Therapy, course of disease


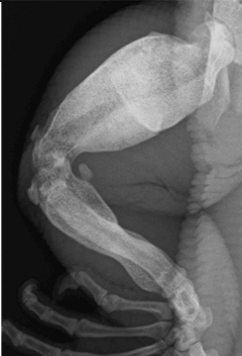
Due to the severe clinical presentation the animal was taken in for intensive care and received cholecalciferol (680 IE/kg p.o., Oleovit D3 Tropfen®, Fresenius Kabi Austria GmbH, Graz, Austria) once, Ringer's solution (20 ml/kg q24h s.c., Ringer-Infusionslösung®, B. Braun Melsungen AG, Melsungen, Deutschland) with Calciumgluconat and Calciumsaccharat (100 mg/kg q24h s.c., Calcium "Fresenius"®, Fresenius Kabi Austria GmbH, Graz, Austria) and Meloxicam (2.4 mg/kg q24h s.c., Metacam 2 mg/ml®, Böhringer Ingelheim (Schweiz) GmbH,

Basel, Schweiz) for seven days and 0.7 ml Calcium “Fresenius” p.o. q24h for further five weeks. The animal was housed in a quarantine terrarium with a new Reptiles Expert UVB 70 W lamp. As it had troubles moving which included proper food intake on it’s own, it was offered soft fruits, mainly grapes, daily at first and fed 2 ml EmerAid Carnivore Care® once a day additionally. The tegu’s physical condition improved slowly but steadily during the following days and after four days it was able to eat dismembered mice on it’s own and to push it’s body up from the ground for the first time. A first blood chemistry control one week after initial presentation the ionized calcium as well as the Ca : P ratio had increased noticeably (Tab. 4). When the tegu was able to feed independently about a week later it was offered a varied diet of fruits (grapes, apples, melons), vegetables (paprika, cucumber, zucchini), insects (mealworms, crickets, grasshoppers) and dismembered mice every second day.

On January 15th 2018 a follow-up blood chemistry showed a noticeable increase in ionized calcium and total calcium levels (see table 4) as well as an increased total Ca : P ratio of 1.7 : 1. On January 24th the animal was given to a foster home in so far good general health, good food intake and slowly progressive agility.

The results of physical examination, type of performed diagnostic imaging, main localization of skeletal changes, results of densitometry, as well as important additional information and if available total calcium, ionized calcium and phosphorus on three occasions are summarized in table 7.

Tab. 7. Overview of clinical and diagnostic imaging history of animal ID 3

Date of presentation	December 2017	January 2018	November 2019
Reason for presentation	poor general condition, swelling of all four limbs	stationary patient follow-up examination	follow-up examination
Physical examination	massive, painful soft tissue swelling of all four limbs, ribs, tail base, locomotion disability, tremor	known alterations, slowly progressive agility, normal behaviour	limb swellings still present, limited range of motion, otherwise active and unimpaired
Total calcium (mmol/L) (3.04 ± 0.2)* (mg/dL) (12.2 ± 0.8)*	1.54 6.17	2.24 8.96	not evaluated
Ionized calcium (mmol/L) (1.0 ± 0.49)** (mg/dL) (4.0 ± 1.97)**	0.64 2.56	0.77 3.09	not evaluated
Phosphorus (mmol/L) (1.8 ± 0.68)* (mg/dL) (5.6 ± 2.1)*	1.63 5.05	1.32 4.09	not evaluated
Performed diagnostic imaging	radiography, CT	-	radiography, CT
RX / CT main locations	humeri, radii, ulnae, femora, tibiae, fibulae, ribs, cervical vertebrae, tail	-	all known pathological changes
Figure (left femur)		-	
Figure type	radiography	-	radiography
Densitometry	vertebrae: up to 714HU	-	vertebrae: up to 1566HU
Additional information	-	-	improved diet and husbandry
Further findings	missing teeth, reduced bone mineralization	-	well mineralized skeleton, formations have smoothed and organized, mineral dense material in GIT

(Reference values \*Carpenter 2018, \*\*ZIMS 2021)

After nearly two years the follow-up CT images and radiographs showed that the skeleton was generally very well mineralized and that the missing teeth had all grown back. At that time the animal was housed in a 2.2 m x 1.4 m x 1.4 m terrarium with one Reptiles Expert UVB 150 W Flood HID-lamp (3 months old, UV index 5.2 at animal height, measured with a Solarmeter® 6.5R Reptile) and one Reptiles Expert UVB 70 W Spot HID-lamp (5 months old, UV index 4.3 at animal height, measured with a Solarmeter® 6.5R Reptile) for UV B provision with a daily exposure time of 10 hours during winter and 12 hours during summer. Additionally, the animal was offered another basking spot with an Osram Vitalux 300 W (5 months old, UV index 7.0

at animal height, measured with a Solarmeter® 6.5R Reptile) for an hour per day. It's diet consisted of alternating mixes of vegetables (paprika, cucumbers, zucchinis) and fruits (apples, bananas, melons, pears, grapes, seasonal berries, mangos) supplemented with herpetal Mineral® twice a week, live insects (subadult and adult grasshoppers, adult crickets and roaches) once a week, chopped chicken hearts once a week, one adult mouse every second week and sprats and raw or boiled eggs from time to time.

When evaluating the radiographs and CT recordings, it was clearly evident that all familiar formations on the long bones had not receded, however, they had smoothed and organized with the underlying bone and were now relatively homogeneously bone-dense (Fig. 1, F and Fig. 2, C).

The humeri had narrowed, partly hyperdense medullary cavities, although it was mostly impossible to determine what exactly the ossified medullary cavity or the expanded compacta was (Fig. 3, H). Both radii were still severely deformed and the former distal articular surface could not be identified. The medullary cavity of the left radius was narrowed to 0.8 mm in diameter and highly hyperdense, while the medullary cavity of the right radius could not be identified at all.

Both ulnae showed slightly opacified medullary cavities.

The medullary cavities of both femora, which were still heavily misshapen, appeared narrow and centrally located. It was not possible to distinguish between ossified medullary cavity and expanded compacta in large areas. Both tibiae displayed an hourglass-shaped deformation of the bone at the distal and proximal diaphysis/metaphysis with less extensive changes in the middle of the diaphysis. Both medullary cavities seemed to be either narrowed or it was not possible to clearly determine what was ossified medullary cavity and expanded compacta.

Some of the ribs were expanded up to 6 mm width. A fusion of four ribs over a length of 23 mm was visible on the left side, which had to be a new formation as this change had not been visible on the previous images (Fig. 1, F). This was rather surprising as the massive fusion occurred in a part of the skeleton which is normally involved in the animal's movement a lot. The cervical vertebrae 1-6 were completely fused and no intervertebral space could be identified (Fig. 5, E, F). The formation ventrally to the cervical spine had dimensions of up to 9.8 mm x 21.2 mm, which is about 2.6 times as high and 2.9 times as wide as the vertebral body of the unaffected seventh cervical vertebra.

At the moment (July 2022), the animal is still doing well despite a few restrictions due to the limb deformations, fused vertebrae and rib fusion.



## 6. Discussion

In reptiles several manifestations of MBDs, ranging from nutritional and husbandry-related diseases like secondary hyperparathyroidism and fibrous osteodystrophy, to non-nutritional related diseases like osteopetrosis, hypertrophic osteodystrophy, hypertrophic osteopathy (acropachy), Paget's disease (osteitis deformans) and panosteitis, have been described in the current literature (Juan-Sallés and Boyer 2020), with NSHP being the most common (Knafo 2019). Besides many case reports describing corresponding clinical pathologies, only quite few literature sources about MBD include histopathological and diagnostic imaging findings to this day (Rotschild et al. 2012, Hoby et al. 2010, Knafo 2019, Rendle and Calvert 2019). In the two presented cases several expectations of findings for MBD described in literature concerning clinical presentation, blood chemistry values and radiographic findings were met and some were not.

The **clinical symptoms** in both animals, especially muscle tremors (Mariani 2007), disability to raise the trunk off the ground, apathy (Boyer and Scott 2019), swollen limbs and the lack of growth (Boyer and Scott 2019) in animal ID 3 (assuming that the reported age is correct) were consistent with the typical symptoms for severe NSHP described in literature. Both animals also showed limb tremors in a direct correlation with ionized calcium levels  $<0.9$  mmol/l which are commonly attributed to clinical hypocalcemia (Rendle and Calvert 2019). But swollen limbs can also be indicative for other underlying diseases like hypertrophic osteopathy, abscesses, edema, neoplasia, osteomyelitis or fractures (Knafo 2019, McCracken et al. 2017). However, especially bilateral symmetrical limb swelling in combination with tremors of the extremities is highly suggestive for either RSHP or NSHP. RSHP is less likely than NSHP to appear in young reptiles (Klaphake 2010) but can nevertheless occur in all age groups when a severe underlying renal pathology is present in the patient. In case of animals ID 1 and ID 3 no radiographic or blood chemistry indications were clearly indicative for causal renal pathology. Hypoproteinemia due to protein losing enteropathy or chronic hepatopathy is another reason for hypocalcemia in reptiles (Boyer and Scott 2019). As total protein was within reference values in both animals this pathologic genesis was ruled out. Low total protein within the reference margin in animal ID 3 might be attributed to its malnourished condition (Heatley

and Russell 2019). In animal ID 1 also bile acid which is used to assess hepatic function was clearly below 60  $\mu\text{mol/L}$ , which is considered the threshold for hepatic dysfunction for fasted animals (Heatley and Russell 2019). Therefore hepatic pathology was deemed unlikely. Due to the animals' relatively young age and a history of bad or unknown dietary and husbandry circumstances in both animals, NSHP was deemed the most likely, but not definite diagnosis in both hereby presented cases.

In case of animal ID 3, the strong correlation of clinical symptoms and **blood chemistry** values, especially the low ionized calcium and low total calcium (Knotek et al. 2003, ZIMS 2021, Gibbons 2013, Eatwell 2009, Eatwell 2007, Eatwell 2010) as well as an inverse total Ca : P ratio at initial presentation underlines the severity of the animal's condition. Both total and ionized calcium are normally kept within normal limits until bone calcium reserves are depleted. Ionized calcium level seldom decreases until terminal as it is crucial for various cell mechanisms (Boyer and Scott 2019). So a condition like the documented must be classified as potentially life threatening. As ionized calcium is the active form of calcium with higher clinical significance (Rendle and Calvert 2019) it should be standard for cases with suspected calcium metabolism-related disorders to always include it in blood chemistry evaluation. In case of animal ID 1 the importance of ionized calcium as a marker for the overall calcium metabolism situation is well pronounced. Despite severe clinical signs (tremors) and a severely low level of ionized calcium total calcium as well as phosphorus were both still within reference margins. Furthermore, the fact that the specimens ID 4, 5 and 10 that did not display any clinical symptoms and had well mineralized skeletons but showed similar or even lower total calcium and phosphorus levels and total Ca : P ratios than the two animals affected by metabolic bone pathologies, emphasizes the key role of ionized calcium as a crucial diagnostic value. It is interesting to note that although animal ID 3 was treated with oral calcium after initial presentation its' ionized calcium level increased at first and then decreased despite the therapy continuing the same way and the animal improving clinically. The administration of oral vitamin D3 not only as a single initial dose but repeatedly as recommended in literature (Carpenter 2018) might be assumed a reason as the animal was in very bad physical condition. Therefore it might not have been sufficiently able to use the UV-B source for "sun-bathing" due to its immobility. Unfortunately, there are no blood chemistry values after the one month

the tegu stayed available that would allow a closer investigation of more long-term blood chemistry development.

However, as there were neither ionized calcium values available from other than the two obviously by MBD affected specimens nor ionized calcium values from the last follow-up examinations of these two animals, it is difficult to discuss whether a direct correlation between ionized calcium levels and skeletal mineralization can be made. Other than that it is possible to assume based on the available information about UV B-provision and diet of the clinically not MBD affected control animals that the provision of proper UV-B light, calcium supplementation and a varied diet (as it was the case in all other animals included in this study) can be considered causative for normal total calcium and phosphorus values in combination with good skeletal mineralization.

**Radiographically**, several expected radiographic signs considered typical for NSHP were documented whereas others were not found in either of the two specimens affected by MBD. In dogs and cats, typical radiologic findings in cases of NSHP include decreased bone opacity, abnormally thin cortices and reduced bone opacity in severely affected animals. Also, deformation of the spine and pathologic folding fractures of the appendicular as well as the axial skeleton are frequently encountered. In extraordinary severe cases of hyperparathyroidism hyperplasia of fibrous tissue, so-called fibrous osteodystrophy, may occur after demineralization of the bones (Pollard and Phillips 2018).

In reptiles, generally reduced bone mineralization, scoliosis of the tail, thinning or even thickening of the long bone cortices, long bone bowing, folding fractures in juvenile and pathologic fractures in adult animals as well as asymmetrical distribution of periosteal new bone are described as major radiographic signs for NHSP (Barten 2000, Hoby et al. 2010, Boyer and Scott 2019, Rendle and Calvert 2019). In lizards bone density is more easily assessed on the limbs. Long bones should be clearly visible with well-defined cortical and medullary areas (Pees 2010a). In this context it is interesting to note that at initial presentation of animal ID 3 the bone density appeared normal based on the seemingly normal to high mineralization of the spine and the ability to properly delineate the transversal processus of the caudal vertebrae from the surrounding soft tissue on the radiographs (Rendle and Calvert 2019). The severely reduced

general bone density detected by the follow-up CT-evaluation may highlight the importance of CT scans as a more sensitive tool for evaluation of bone density.

The radiographically diagnosed bilateral swellings of the limbs as well as the scoliosis of the tail, the initially generally reduced cortical bone density and the expanded compacta in animal ID 3 are consistent with previous findings in cases of NSHP (Rendle and Calvert 2019). Furthermore the asymmetrical distribution of periosteal new bone formation and the cortical ballooning are reported radiographic signs attributed to secondary hyperparathyroidism (SHP) (Barten 2000). In contrast the radiographic changes in animal ID 1 did not affect the limbs, as noted in the literature (Juan-Sallés and Boyer 2021), but the ribs initially and progressed to the limbs in the further course of the disease. However, it is possible that both pathologies are not directly linked to each other and developed independently. It seems remarkable that especially thickening or ballooning of the long bone cortices is not described in dogs or cats as a roentgen sign for SHP (Stander and Cassel 2016).

Possible new findings for MBD in the two cases include several radiographic alterations that have not been described either at all or not to this severe extent in literature yet. Especially the assumed progressive mineralized formation ventral to the cervical spine in animal ID 3 and the progressive new bone formation along the ribs of both animals do not meet any specific descriptions given in current literature about MBDs in reptiles. There are several clues about slightly similar paradoxical mineralizations related to normal or low vitamin D and calcium levels in published papers but these report primarily calcification of organs and blood vessels (Raiti and Garner 2006, Raiti 2019), so the exact pathogenesis for the paradoxical mineralization in the presented cases remains unclear until definite further findings. A metastatic calcification due to hypercalcemia can be ruled out due to the obvious hypocalcemia evident in animal ID 3 (Schenck et al. 2012, Harr et al. 2001, Ferguson et al. 2009).

The smoothly delineated, presumably periosteal reactions observed in the long bones can be classified as continuous and solid appositions to the underlying cortex rather than initial replacements. This is characteristic of non-aggressive, benign bone lesions (Ludewig and McEvoy 2006). The overall intactness of the cortices and the distinct transition zone of the lesions also support this assumption (Thrall 2018). The commonly described definite thinning of the long bone cortices in NSHP or RSHP (Zotti et al. 2004) could not be observed in the

examined cases. However, there seem to exist controversial opinions about cortical bone changes related to NSHP in reptiles. Besides the frequently cited cortical thinning there are also authors who consider cortical thickening a crucial radiographic sign for NSHP (Rendle and Calvert 2019). Some authors even describe both pathological cortical thickening of long bones due to extensive periosteal hyperostosis and cortical thinning due to decalcification as possible radiographic presentations of MBDs, depending on the affected animal's age (Pees, 2010b). In young, growing animals hypocalcemia is likely to lead to cortical bone distention whereas in adult animals demineralization is reported to cause cortical thinning (Pees 2010a). Tegu ID 1 and ID 3 were subadult (with a life expectancy of 15-20 or more years) at the time of onset of clinical symptoms which would support this hypothesis.

Both the supposed soft tissue mineralization, the histologically confirmed new bone tissue formation and the radiographic changes evident in the long bones partly fit several possible **differential diagnoses**. Especially the voluminous new bone formations below the cervical spine of animal ID 3 and around the ribs of both animals resemble some typical presentations, localization, progressive course and age of affected animals of osteochondromatosis (Dennis et al. 2001, Seiler et al. 2011). Neoplasia of other genesis as an initial potential differential diagnosis of the rib alteration could not be entirely ruled out solely based on the radiographic findings (Saunders et al. 2011), but later on at least in animal ID 1 due to the pathohistological results. Whereas histological findings in osteochondromas would include a typical capping of mature cartilaginous tissue and bone marrow cells as well as a lack of osteoblasts (Caporn and Read 1996, Pollard and Phillips 2018, Thompson and Dittmer 2017) histopathological findings made in animal ID 1 revealed a high quantity of osteoblasts and no sign of cartilaginous capping.

Although the new bone formation along the cervical spine and ribs may also appear similar to findings in cats suffering from severe hypervitaminosis A (Allan and Davies 2018), such bony changes have not been reported in reptiles so far. Furthermore, none of the clinical symptoms associated with hypervitaminosis A in reptiles like edema, severe ecdysis, dermatitis or skin sloughing (Juan-Sallès and Boyer 2021) were present in either of the two animals, so it was ruled out as differential diagnosis.

The progressively increasing bone density of the medullary bone of the spines of both animals (as well as in the specimens ID 4 and ID 10 included in this study) shows typical features of osteopetrosis (Pollard and Phillip 2018). However, the histopathological findings in animal ID 1 do not meet the typical presentation of osteopetrosis which is characterized by a constant decrease in osteoclasts and correlated reduced bone absorption (Ocarino 2008). Since there were no samples taken from the other three animals for histopathologic examination, for them osteopetrosis cannot be completely excluded as a potential differential diagnosis.

On the other hand, the quite evenly distributed, massive periosteal reaction on the long bones may serve as a radiographic sign of hypertrophic osteopathy, where long bones can show extensive, uniform to palisade-like periosteal hyperostosis, usually sparing the joint spaces (Pees 2010b). The latter could be ruled out by the absence of a neoplastic mass or severe chronic inflammatory process and the improvement in clinical symptoms along with calcium substitution. In young dogs of medium to giant breeds similar radiographic signs of metaphyseal cortical thickening may be attributed to hypertrophic osteodystrophy (HOD), where a typical bilateral, symmetrical and progressive swelling of the metaphyses of the long bones occurs. Another roentgen sign for HOD is the heterogeneous appearance of the metaphyses including a lucent band paralleling the physes (double physes sign) (Pollard and Phillips 2018). Such a radiographic sign was not present in the tegus.

A much rarer possible differential in dogs, more precisely young West Highland White Terriers, is craniomandibular osteopathy (CMO), which primarily affects the mandibula, tympanic bullae and occipital bone but may also cause proliferative remodeling and enlargement of long bone diaphyses and/or metaphyses (Stander and Cassel 2016). However, neither the clinical symptoms nor the overall radiological findings are clearly indicative for any of the named disease complexes. The suspected diagnosis secondary hyperparathyroidism in both animals was made based on the clinical presentation at the time of the onset of typical symptoms, corresponding blood chemistry values, especially ionized calcium, medical history, several matching radiographic findings and the improvement of the animals' condition under calcium substitution and improvement of husbandry and diet. Due to the inconclusive radiographic findings it is also possible that there is not one but there are multiple underlying pathophysiologies of the skeletal alterations in both cases.

As both animals are still alive and doing well under the limiting conditions of their misshapen limbs no thorough pathological examination, which would be considered important for histological differentiation and classification of the present skeletal pathologies, has been possible yet. This is for sure one limitation of this retrospective study as only one tissue sample from one of the two animals was histologically examined and therefor a definite classification of all found skeletal and soft tissue changes was not possible. Histologically, fibrous metaplasia replacing poorly mineralized or lytic bone would be expected pathognomonic findings for active fibrous osteodystrophy in secondary hyperparathyroidism (Hoby 2010).

Another diagnostic limitation is that the definitive diagnosis of hyperparathyroidism requires the diagnosis of elevated PTH, but as commercially available mammalian assays seem to lack accuracy for reptiles, plasma calcidiol values are a reliable alternative to assess potential UVB or dietary D3 deficiencies (Eatwell 2008, Selleri and Di Girolamo 2012, Oonincx et al. 2010). Unfortunately, the latter also was not available in the discussed cases, so ionized calcium, total calcium and phosphorus were used to evaluate calcium metabolism related conditions. It is also not entirely clear why there was still a progression of the skeletal changes in animal ID 1 despite the optimization of nutritional and husbandry-related parameters. Oral calcium therapy as recommended in common literature (Boyer and Scott 2019, Carmel and Johnson 2018) and performed with animal ID 3 as addition to the improved husbandry and diet might have improved the animal's condition earlier. It is of course possible that the information given by the in general seemingly trustworthy owner about changes in nutrition and husbandry were not correct or incomplete so that the pathologic condition existed longer than assumed. As it is not clear which types of UV-B lamps the owner used, improper positioning, a too low wattage or UV-B index might have attributed to the lack of health improvement as well as improper supplementation and diet about which also no quantitative information was available. There are also no recordings on enclosure temperatures which play a crucial role for the metabolism and immune system in reptiles and therefor can affect existing metabolic conditions in a negative way if the animal is not kept in its' preferred optimal temperature zone (Rossi 2019, Divers 2019, Howerth 2019). It is also remarkable that the progression of the skeletal changes seems to have stopped during the time when the animal started to have permanent access to natural sunlight for most of the year. That not only emphasizes the general need for UV-B provision but underlines the importance for evaluation of the species-specific demand for UV-B (Baines

et al. 2016). As animal ID 3 was initially presented at the clinic at already a very late stage of MBD with severe clinical and radiographic pathologies, it was unfortunately not possible to compare the early stages of the onset of the skeletal changes of both animals for similarities.

Another result of this study that should not be disregarded is the high median bone density (especially of the cortices) in all animals not affected by clinical or radiographic signs of MBD. Even the bone density of the by MBD affected animal ID 1 by far exceeds HU values cited in current literature (Gumpenberger 2011, Pees 2010b) at the second follow-up CT examination. As there are no HU reference values specifically for tegus mentioned in current literature it is possible that a high cortical bone density is generally typical for tegus, but so far, no data from other sources, either published or unpublished (like personal communication), for comparison could be obtained. In order to gain a better insight into this phenomenon effort should be put into gathering more species-specific CT data. Also, PTH, vitamin D3 and other blood chemistry values correlated with MBDs should be obtained from animals which show increased bone mineral density in CT scans to be able to identify possible underlying metabolic mechanisms.

A major difference in the course of disease of animals ID 1 and ID 3 is the development of the medullary bone density. In animal ID 3 the medullary density increased from the initial presentation to the follow-up examination 23 months later. In animal ID 1 it increased between the initial CT scan and the first follow-up examination 16 months later, but decreased in the humeri and femora from the first to the second follow-up examination another 29 months later while the BMD of the spine and skull increased further. The difficult distinction between expanded compacta and ossified medullary cavity in the humeri due to the extensive bone changes at the time of the first follow-up examination and therefor necessary subjective positioning of the ROI measuring points may be a possible reason for a measurement deviation and a reason for this diametral data.

To probably fill some data holes left in this study it should be encouraged to keep track of the animals' development and collect further clinical, radiographical and blood chemistry values when they are presented for follow-up examinations in the future. If possible, when the animals decease, thorough pathologic and histopathologic examinations should be conducted to



determine the exact type of underlying pathology. Considering the findings of this study in the light of the still high importance of thorough investigation to produce scientifically valuable data and reference values for many reptile species, not only the documentation of current cases, but also the processing of old cases with up-to-date knowledge seems desirable in the future. Especially in frequent pathological presentations of reptiles like MBDs, investigation of etiology and pathophysiology should be further supported.

Finally, it seems important to point out that despite the truly severe clinical and radiographic presentation of animal ID 3, which would have justified euthanasia, it was possible with extensive intensive care to improve its condition long-term so that it is able to live with only minimal limitations until today.

## 7. Zusammenfassung

Für eine retrospektive Studie über pathologische Skelettveränderungen bei zehn Individuen von Tegus (*Tupinambis*) wurden CT-Bilder und Röntgenaufnahmen ausgewertet. Die Bilder stammten entweder von Tieren, die an der Klinischen Abteilung für Bildgebende Diagnostik der Veterinärmedizinischen Universität Wien vorgestellt oder Aufnahmen, die zur Zweitmeinung von externen Tierärzten an die Klinik übersandt wurden. Dabei wurden zwei nicht miteinander in Verbindung stehende Patienten mit ähnlichen röntgenologischen Befunden massiver Skelettveränderungen, vor allem der langen Röhrenknochen, insbesondere der Humeri und Femora, der Rippen, aber auch der Wirbel, entdeckt. Die röntgenologisch diagnostizierten Skelettveränderungen ähnelten typischen, bei Reptilien bekannten Knochenveränderungen durch Mineralstoffwechselstörungen (MBD), vor allem sekundärem Hyperparathyreoidismus, zeigten jedoch ein ungewöhnlich hohes Ausmaß an Veränderungen. Bei den Tieren handelte es sich um subadulte *Tupinambis merianae*, die zum Zeitpunkt der pathologischen Röntgenbefunde mit massiven Schwellungen der Gliedmaßen, Unbeweglichkeit und Apathie sowie niedrigem Blutkalziumspiegel vorgestellt wurden. Im direkten Vergleich mit klinisch und röntgenologisch unauffälligen Artgenossen fielen eine teilweise reduzierte Knochendichte, gering- bis hochgradige knöcherne periostale Zubildungen und Mineralisationen der umgebenden Weichteile auf. Nach chirurgischer Entnahme einer rippennahen Masse bei einem der Tiere zeigte die histologische Untersuchung, dass das entfernte Material aus neu gebildetem, regelmäßigem Knochengewebe bestand. Bei beiden Tieren wurde die Entwicklung der Skelettveränderungen und des umgebenden Weichteilgewebes über einen Zeitraum von zwei bzw. vier Jahren regelmäßig kontrolliert und anhand von Röntgenbildern und CT-Aufnahmen dokumentiert. In dieser Zeit konnte festgestellt werden, dass sich unter optimierten Haltungs- und Fütterungsbedingungen die zum Teil massiven Neubildungen an den Röhrenknochen zwar nicht zurückbildeten, aber reorganisiert wurden, während die Veränderungen an den Rippen und Wirbeln tendenziell weiter voranschritten.

## 8. Summary

For a retrospective study on pathologic skeletal changes in ten individuals of tegus (*Tupinambis*), CT images and radiographs were reviewed. The images were either obtained from cases presented at the Clinical Unit of Diagnostic Imaging of the University of Veterinary Medicine Vienna or were sent to the clinic for second opinion from external veterinarians. During the process two unrelated cases with similar radiographic findings of massive skeletal changes of mostly the long bones, especially the humeri and femora, the ribs and also vertebrae were discovered. These skeletal changes most likely resembled bone alterations due to metabolic bone disease, namely secondary hyperparathyroidism, but showed a rarely seen extent of radiographic changes that could be followed over a longer period of time. The animals were both subadult *Tupinambis merianae* which presented with massive swelling of the limbs, immobility and apathy as well as low blood calcium levels. In direct comparison with conspecifics that were clinically and radiographically normal, partly reduced bone density, low to high grade periosteal reactions and suspected mineralizations of the surrounding soft tissues were noticeable. After surgical sampling of a mass near the ribs of one of the animals, histologic examination showed that the removed mass consisted of newly formed, regular bone tissue. In both animals, the development of the skeletal changes and surrounding soft tissue were periodically checked over two and four years and documented radiographically and with CT. During that time it was observed that under optimized housing and feeding conditions, the partly massive formations on the long bones did not recede, yet they got more organized, while the changes affecting the ribs and vertebrae tended to progress further.

## 9. Abbreviations

approx.	approximately
BMD	bone mineral density
BW tegu	black and white tegu
Ca	calcium
CB	captive bred
CMO	craniomandibular osteopathy
CT	computed tomography
dL	deciliter
FB	farm bred
Fig.	figure
g	gram(s)
GIT	gastrointestinal tract
HID	high intensity discharge
HOD	hypertrophic osteodystrophy
HPF	high power field
HU	hounsfield unit(s)
ID	identification number
i.m.	intramuscular
kV	kilovolts
mAs	milliampere seconds
L	liter
M	month(s)
Max	maximum
MBD(s)	metabolic bone disease(s)
MD	median
mg	milligram
mmol	millimole
Min	minimum
MV	mean value

NSHP	nutritional secondary hyperparathyroidism
P	phosphorus
PTH	parathyroid hormone
RSHP	renal secondary hyperparathyroidism
R tegu	red tegu
ROI	region of interest
RX	radiography
s	seconds
s.c.	subcutaneous
SHP	secondary hyperparathyroidism
Tab.	table
WBC	white blood cells
y	year(s)

## 10. Bibliography

Allan G and Davies S. 2018. Radiographic Signs of Joint Disease in Dogs and Cats. *In* Thrall DE (ed.): Textbook of Veterinary Diagnostic Radiology. Elsevier, St. Louis, USA: 421-22.

Baines FM, Chattell J, Dale J, Garrick D, Gill IS, Goetz M, Skelton T, Swatman M. 2016. How much UV-B does my reptile need? The UV-Tool, a guide to the selection of UV lightning for reptiles and amphibians in captivity. *JZAR*, 4(1): 42-63

Barten SL. 2000. What's your diagnosis? Distal leg necrosis in a green iguana, *Iguana iguana*. *J Herp Med Surg*, 10: 48.

Boyer TH, Scott PW. 2019. Nutritional Diseases. *In* Divers SJ, Stahl SJ (eds.): Mader's Reptile and Amphibian Medicine and Surgery (3rd ed). St. Louis, USA: Elsevier, 932-50.

Boyer TH, Scott PW. 2019. Nutritional Secondary Hyperparathyroidism. *In* Divers SJ, Stahl SJ (eds.): Mader's Reptile and Amphibian Medicine and Surgery (3<sup>rd</sup> ed). St. Louis, USA: Elsevier, 1326-7.

Caporn TM, Read RA. 1996. Osteochondromatosis of the cervical spine causing compressive myelopathy in a dog. *J Small Anim Pract*. 37/3: 133-7

Carmel B, Johnson R. 2018. Nutritional and Metabolic Diseases. *In* Doneley B, Monks D, Johnson R, Carmel B (eds.): Reptile Medicine and Surgery in Clinical Practice. Oxford, UK: John Wiley & Sons Ltd, 185-190.

Dennis R, Kirberger R M, Wrigley R H, Barr F J. 2001. Small Animal Radiological Differential Diagnosis. Saunders, London, UK: 3.

Dennis PM, Bennett RA, Harr KE, Lock BA. 2001. Plasma concentration of ionized calcium in healthy iguanas. *J Am Vet Med Assoc*, 219(3): 326-8.

Divers SJ. 2019. Hepatology. *In* Divers SJ, Stahl SJ (eds.): Mader's Reptile and Amphibian Medicine and Surgery (3rd ed). St. Louis, USA: Elsevier, 649-68.

Eatwell K. 2010. Calcium and phosphorus values and their derivatives in captive tortoises (*Testudo* species). *J S An Prac*, 51(9): 472-5.

Eatwell K. 2009. Comparison of total calcium, ionized calcium and albumin concentrations in the plasma of captive tortoises (*Testudo* species). *Vet Rec*, 165(16): 466-8.

Eatwell K. 2008. Plasma concentrations of 25-hydroxycholecalciferol in 22 captive tortoises (*Testudo* species). *Vet Rec*, 162(11): 342-5.

Eatwell K. 2007. Effects of Storage and Sample Type on Ionized Calcium, Sodium and Potassium Levels in Captive Tortoises, *Testudo* spp. *J Herp Med Surg*, 17(3): 84-91.

Ferguson GW, Brinker AM, Gehrman WH, Bucklin SE, Baines FM, Mackin SF. 2010. Voluntary Exposure of Some Western-Hemisphere Snake and Lizard Species to Ultraviolet-B Radiation in the Field: How Much Ultraviolet-B Should a Lizard or Snake Receive in Captivity?. *Zoo Biol* 29(3): 317-34

Ferguson GW, Gehrman WH, Peavy B, Painter C, Hartdegen R, Chen TC, Holick MF, Pinder J E. 2009. Restoring Vitamin D in Monitor Lizards: Exploring the Efficacy of Dietary and UVB Sources. *J Herp Med Surg*, 19(3): 81-88.

Gibbons PM, Klaphake E, Carpenter JW. 2013. Reptiles. *In* Carpenter JW (ed.): Exotic Animal Formulary (4th ed). St. Louis, USA: Elsevier, 83-182.

Gramanzini M, Di Girolamo N, Gargiulo S, Greco A, Cocchia N, Delogu M, Rosapane I, Liuzzi R, Selleri P, Brunetti A. 2013. Assessment of dual-energy x-ray absorptiometry for use in evaluating the effects of dietary and environmental management on Hermann's tortoises (*Testudo hermanni*). *Am J Vet Res*, 74(6): 918-924.

Gumpenberger M. 2011. Chelonians. *In* Schwarz T, Saunders J (eds.): Veterinary Computed Tomography. Chichester, UK: Wiley-Blackwell, 533-544.

Harr KE, Alleman AR, Maxwell LK, Lock BA, Bennett RA, Jacobson ER. 2001. Morphologic and cytochemical characteristics of blood cells and hematologic and plasma biochemical reference ranges in green iguanas. *J Am Vet Med Assoc*, 218(6): 915-21.

Heatley JJ, Russell KE. 2019. Clinical Chemistry. *In* Divers SJ, Stahl SJ (eds.): Mader's Reptile and Amphibian Medicine and Surgery (3rd ed). St. Louis, USA: Elsevier, 319-32.

Hedley J, Kubiak M. 2015. Neurologic Diseases of Birds and Reptiles. *J Exot Pet Med*, 24(1): 6-20.

Hoby S, Wenker C, Robert N, Jermann T, Hartnack S, Segner H, Aebischer C-P, Liesegang A. 2010. Nutritional metabolic bone disease in juvenile veiled chameleons (*Chamaeleo calyptratus*) and its prevention. *J Nutr*, 140(11): 1923-31.

Howerth EW. 2019. Immunopathology. *In* Divers SJ, Stahl SJ (eds.): Mader's Reptile and Amphibian Medicine and Surgery (3rd ed). St. Louis, USA: Elsevier, 356-64.

Juan-Sallés C, Boyer TH. 2021. Nutritional and Metabolic Diseases. *In* Garner MM, Jacobson ER (eds.): Noninfectious Diseases and Pathology of Reptiles: Color Atlas and Text. Boca Raton, USA: CRC Press, 55-105.

Kiefer I, Pees M. 2010. Computed tomography (CT). *In* Krautwald-Junghans M, Pees M, Reese S, Tully T (eds.): Diagnostic Imaging of Exotic Pets. Hannover, Germany: Schluetersche, 358-333.

Klaphake E. 2010. A Fresh Look at Metabolic Bone Diseases in Reptiles and Amphibians. *Vet Clin North Am Exot Anim Pract*, 13(3): 375-392.



- Knafo S E. 2019. Musculoskeletal System. *In* Divers SJ, Stahl SJ (eds.): Mader's Reptile and Amphibian Medicine and Surgery (3rd ed). St. Louis, USA: Elsevier, 894-916.
- Knotek Z, Knotkova Z, Doubek J, Pejrilova S, Hauptman K. 2003. Plasma Biochemistry in Female Green Iguanas (*Iguana iguana*) with Calcium Metabolism Disorders. *Acta Vet*, 72: 183-9.
- Köhler G, Langerwerf B. 2000. Tejus: Lebensweise, Pflege, Zucht. Offenbach, Germany: Herpeton, 52.
- Ludewig E, McEvoy FJ. 2006. Basics of musculoskeletal radiography and radiology. *In* Barr FJ, Kirberger RM (eds.): BSAVA Manual of Canine and Feline Musculoskeletal Imaging. Quedgeley, UK: BSAVA, 12.
- Mariani CL. 2007. The neurologic examination and neurodiagnostic techniques for reptiles. *Vet Clin North Am Exot Anim Pract*, 10(3): 855-91.
- McCracken H, Carmel B, Chitty J, Doneley B, Johnson R, Lennox AM, Monks D, Olsson A. 2017. Differential Diagnosis: A Problem-based approach. *In* Doneley B, Monks D, Johnson R, Carmel B (eds.): Reptile Medicine and Surgery in clinical practice: 217-53.
- Ocarino NM, Goulart C E, Falci S M, Souza P C, Serakides R. 2008. Osteopetrosis and osteonecrosis in snake Boa constrictor. *Arq Bras Med Vet Zootec*, 60(5): 1284-1287.
- Ooninx DGAB, Stevens Y, van den Borne JJGC, van Leeuwen JPTM, Hendriks WH. 2010. Effects of vitamin D3 supplementation and UVb exposure on the growth and plasma concentration of vitamin D3 metabolites in juvenile bearded dragons (*Pogona vitticeps*). *Comp Biochem Physiol B Biochem Mol Biol*, 156(2): 122-8.
- Pees M. 2010a. Radiographic investigation. *In* Krautwald-Junghans M, Pees M, Reese S, Tully

T: Diagnostic Imaging of Exotic Pets. Hannover, Germany: Schluetersche, 310-333.

Pees M. 2010b. Special diagnostics, pathological findings. In Krautwald-Junghans M, Pees M, Reese S, Tully T (eds.): Diagnostic Imaging of Exotic Pets. Hannover, Germany: Schluetersche, 378-93.

Pollard RE, Phillips KL. 2018. Orthopedic Diseases of Young and Growing Dogs and Cats. In Thrall DE (ed.): Textbook of Veterinary Diagnostic Radiology. St. Louis, USA: Elsevier, 348-65.

Preziosi R, Diana A, Florio D, Gustinelli A, Nardini G. 2007. Osteitis deformans (Paget's disease) in a Burmese python (*Python molurus bivittatus*) – a case report. Vet J, 174(3): 669-72.

Raiti P, Haramati N. 1997. Magnetic resonance imaging and computerized tomography of a gravid leopard tortoise (*Geochelone pardalis pardalis*) with metabolic bone disease. J Zoo Wildl Med, 28(2): 189-197.

Raiti P, Garner M. 2006. Metastatic Mineralization in a Geoffrey's Side-Necked Turtle, *Phrynops geoffroanus*. J Herp Med Surg, 16(4): 135-9.

Raiti P. 2019. Non-invasive imaging. In Girling S J, Raiti P (eds.): BSAVA Manual of Reptiles (third edition). Gloucester, UK: BSAVA, 134-159.

Reece RL, Dickson DB, Butler R. 1986. An osteopetrosis-like condition in a juvenile rhinoceros iguana (*Cyclura cornuta*). Aust Vet J, 63(10): 343-4.

Reese AM. 1923. The osteology of Tegu, *Tupinambis nigropunctatus*. J o morph, 38(1): 1-17

Rendle M, Calvert I. 2019. Nutritional problems. In Girling S J, Raiti P (eds.): BSAVA Manual of Reptiles (third edition). Gloucester, UK: BSAVA, 365-396.

Rossi JV. 2019. General Husbandry and Management. *In* Divers SJ, Stahl SJ (eds.): Mader's Reptile and Amphibian Medicine and Surgery (3rd ed). St. Louis, USA: Elsevier, 109-30.

Rothschild B, Schultze HP, Pellegrini R. 2012. Summary of Osseous Pathology in Amphibians and Reptiles. *In* Rothschild BM, Schultze HP, Pellegrini (eds.): Herpetological Osteopathology. New York, USA: Springer-Verlag, 11-53.

Saunders J, Vignoli M, Gielen I. 2011. Thoracic Boundaries. *In* Schwarz T, Saunders J (eds.): Veterinary Computed Tomography. Chichester, UK: Wiley-Blackwell, 285-296.

Schenck PA, Chew DJ, Nagode LA, Rosol TJ. 2012. Disorders of Calcium: Hypercalcemia and Hypocalcemia. *In* DiBartola S (ed.): Fluid, Electrolyte, and Acid-Base Disorders in Small Animal Practice. St. Louis, USA: Elsevier, 120-94.

Seiler G, Kinns J, Dennison S, Saunders J, Schwarz T. 2011. Vertebral column and spinal cord. *In* Schwarz T, Saunders J: Veterinary Computed Tomography. Chichester, UK: Wiley-Blackwell, 217.

Selleri P, Di Girolamo N. 2012. Plasma 25-hydroxyvitamin D3 concentrations in Hermann's tortoises (*Testudo hermanni*) exposed to natural sunlight and two artificial ultraviolet radiation sources. *Am J Vet Res*, 73(11): 1781-6.

Silverman S. 2006. Diagnostic imaging. *In* Divers SJ, Stahl SJ (eds.): Mader's Reptile and Amphibian Medicine and Surgery (2nd ed). St. Louis, USA: Elsevier, 471-489.

Stander N, Cassel N. 2016. Long bones – juvenile. *In* Kirberger RM and McEvoy FJ (eds.): BSAVA Manual of Canine and Feline Musculoskeletal Imaging (2<sup>nd</sup> edition). Quedgeley, UK: BSAVA, 87-107.

Thompson KG, Dittmer KE. 2017. Tumors of Bone. *In* Meuten DJ (ed.): Tumors in Domestic

Animals (5<sup>th</sup> edition). Hoboken, USA: John Wiley & Sons: 356-424

Thrall DE. 2018. Principles of Radiographic Interpretation of the Appendicular Skeleton. *In* Thrall DE (ed.): Textbook of Veterinary Diagnostic Radiology. St. Louis, USA: Elsevier, 334-347.

Troiano J, Gould E, Gould I. 2008. Hematological reference intervals in Argentine lizard *Tupinambis merianae*. *Comp Clin Path*, 17: 93-97

Williams J. 2002. Orthopedic radiography in exotic animal practice. *Vet Clin North Am Exot Anim Pract*, 5(1): 1-22.

Zotti A, Selleri P, Carnier P, Morgante M, Bernardini D. 2004. Relationship between metabolic bone disease and bone mineral density measured by dual-energy x-ray absorptiometry in the green iguana (*Iguana iguana*). *Vet Radiol Ultrasound*, 45(1): 10-16.

ZIMS. *Salvator merianae*/Argentine black and white tegu – chemistry/fluid analysis. Available from: Species 360. Accessed 2021 Sep 09.

ZIMS. *Salvator merianae*/Argentine black and white tegu – chemistry/fluid analysis. Available from: Species 360. Accessed 2022 Jun 24.

## 12. List of figures / tables

**Figure 1:** Comparative dorsoventral radiographs of three different tegus. **A** represents the normal reference animal (ID2) with well mineralized slim long bones without any periosteal new bone formations. **B**, **C** and **D** represent tegu ID 1 from 13.6.2016, 15.1.2018 and 15.6.2020, respectively, while **E** and **F** are tegu ID 3 from 14.12.2017 and 5.11.2019. The bony changes are described in detail in the individual case reports. It is remarkable that the changes of the cervical spine in tegu ID 3 are also seen on these dorsoventral radiographs

**Figure 2:** Comparative 3D CT reconstruction of three tegus. **A** is the reference tegu ID 2, **B** is tegu ID 1 from 15.01.2018 and **C** is tegu ID 3 from 05.11.2019. In **B** the massive, bullous changes of the humeri and radii are clearly visible as well as the new formations affecting both femora of animal ID 1. **C** is from a follow-up examination of animal ID 3 with pronounced re-organized and smoothed long bones. Note the extensive alterations of the ribs in both **B** and **C**.

**Figure 3:** Comparative multiplanar reconstructions of CTs in bony window of three different tegus, **A** (left front limb) and **B** (both hind limbs) coronal plane, **C** and **D** (both front legs) transverse (body) /sagittal (humerus) plane aligned to fit the body region shown, **E** to **H** transverse plane of the left humerus. **A** and **B** represent tegu ID 1, **C**, **D**, **F**, **G** and **H** represent tegu ID 3 (**C**, **D**, **F** and **G** from 14.12.2017 and **H** from 5.11.2019) and **E** is the normal reference animal ID 2. Note the bullous alterations and swelling of the right humerus with up to twice its original diameter extending over the entire diaphysis in **A** with a generalized hyperdense medullary cavity which makes it nearly impossible to distinguish between a seemingly expanded cortical or maybe ossified medullary bone in most areas. In **B** there are similar bilateral changes visible in the femora, which display bullous swelling that enclose the bones in the area of the distal diaphysis. The cortical bone appears intact and displays no changes, while up to 5mm high and solid (left leg) and 6mm high and cloudy (right leg), smoothly demarginated, relatively homogeneously bone-dense periosteal reactions with densities up to 400 HU were discovered. The medullary cavity presented irregularly compacted. In **C** and **D** both humeri display massive cloudy smoothly demarginated swellings of presumably periosteal origin with heterogenous density of about three times the bone

diameter. Medullary cavities are partly indistinguishable from the compacta. In **F** and **G** the cloudy, heterogenous, but mostly smoothly demarginated appearance of the changes of the left humerus of animal ID 3 is clearly visible. In **H** the bony alterations are now visibly condensed and smoothed. It is not clearly distinguishable what is massively narrowed, respectively mostly ossified medullary cavity or expanded compacta although the highly hyperdense, thin outline of the bone may represent the compacta. In comparison a clear distinction between hypodense medullary cavity, hyperdense cortical bone and surrounding soft tissue is possible in **E**.

**Figure 4:** Subadult *Tupinambis merianae* with pronounced swelling of all four limbs

**Figure 5:** Comparative multiplanar reconstructions of the CTs in bony window of the head and cervical spine of two different tegus, **A**, **C** and **E** in sagittal and **B**, **D** and **F** in transverse plane. **A** and **B** represent tegu ID 2 and **C** to **F** represent tegu ID 3 (**C** and **D** from 14.12.2017 and **E** and **F** from 5.11.2019). There are severe, at first more spongy and later on more solid new bone formations ventral at the cervical vertebrae in the affected animal ID 3. Note the overall reduced bone density of the diseased animal (ID 3) in comparison to the healthy reference animal (**A** and **B**). However, the density improved from 2017 to 2019.

**Table 1:** Animal data of nine black and white tegus (*Tupinambis merianae*) (BW tegu) and one red tegu (*Tupinambis rufescens*) (R tegu) at initial presentation

**Table 2:** Diagnostic imaging methods, presence of abnormal radiographic findings, type of radiographic pathology at initial presentation and carried out follow-up examinations

**Table 3:** Mean ( $\pm$  SD) and range of bone mineral density of six specimens

**Table 4:** Ionized calcium, total calcium, phosphorus and total Ca : P ratio of six specimens

**Table 5:** Overview of clinical and diagnostic imaging history of animal ID 1

**Table 6:** Hematology of animal ID 3 at initial presentation

**Table 7:** Overview of clinical and diagnostic imaging history of animal ID 3